UNIVERSIDADE FEDERAL DO RIO GRANDE DO SUL
INSTITUTO DE INFORMÁTICA
PROGRAMA DE PÓS-GRADUAÇÃO EM COMPUTAÇÃO

RENAN SALES BARROS

Simulation of Human Skin Pigmentation Disorders

Thesis presented in partial fulfillment
of the requirements for the degree of
Master of Computer Science

Prof. Dr. Marcelo Walter
Advisor

Porto Alegre, March 2013

AGRADECIMENTOS

Essa mensagem vai ser bastante pessoal e, por isso, eu não pretendo incluir o sobrenome dessas pessoas. Aqueles aos quais esses agradecimentos se referem saberão que a mensagem é para eles o que, na minha visão, é o mais importante.

Eu achava que dessa vez, pela grande distância separando a gente, a minha família teria um impacto menor no meu mestrado. Felizmente, eu estava errado. Ellton, publicar um trabalho contigo durante esse mestrado foi uma experiência muito boa. E você ainda conseguiu toda a verba pra eu ir apresentar o trabalho. Não é todo mundo que tem um irmão mais novo como você. Nayara, o trabalho em conjunto que fizemos me ajudou a tirar uma boa nota em uma das disciplinas, também foi ótimo fazer esse trabalho contigo. Meus pais então, apesar do raro convívio que tivemos, os bons momentos que partilhamos me faziam retornar renovado pra minha rotina. A todos vocês, muito obrigado .

Marcelo Walter, eu não consigo me imaginar tendo sido orientado por outra pessoa, eu não te vejo apenas como um orientador, mas também como um amigo. Nós conseguimos achar um jeito bom de trabalhar. Espero que a gente desenvolva mais trabalhos no futuro. Muito obrigado pela parceria durante esse mestrado.

E o que dizer sobre meus colegas de laboratório, vocês foram uma segunda família que me apoiou e que também puxou minha orelha quando necessário. Rosália, na nossa primeira conversa eu era cobaia de uma das tuas experiências, de lá pra cá, não consigo contar quantas experiências a gente passou nem imaginar quantas a gente ainda vai passar. Teus conselhos foram muito valiosos, muito obrigado por ser essa amiga que hoje não sei viver sem. Vinicius, você foi a pessoa mais positiva e compreensiva com quem eu tive o prazer de conviver. Você sempre tentou me mostrar que sou capaz de superar todos os desafios. Muito obrigado por tudo. André, quantas caminhadas, visitas ao Cavanhas, churros na Redenção e discussões a gente teve. Tive que exercitar muito a minha habilidade de organizar e defender ideias contigo, muito obrigado cara, até pelas piadas. Muito obrigado também a Tati, Jerônimo, Marcos, Lenna, Marcelinho, Fred, Bernardo e todos os outros membros do Laboratório com quem eu dividi esses dois anos de pesquisa e que me ajudaram de alguma forma.

Por último, mas de forma alguma menos importante, meu muito obrigado pras minhas amigas Letícia e Carina. Obrigado por vocês estarem disponíveis pra tirar minhas dúvidas sobre matemática, por sorte, eu acho que sempre acabava resolvendo tudo sozinho então sobrava mais tempo pra pipoca e corridas na Redenção, né Letícia; ou pra dançar salsa e me aventurar dando uma de copiloto, né Carina.

A todas essas pessoas, meu muito obrigado,

Renan Sales Barros

CONTENTS

LIST OF ABBREVIATIONS AND ACRONYMS

BRDF   Bidirectional reflectance distribution function

BMI   Body mass index

FFM   Fat-free mass

IGH   Idiopathic guttate hypomelanosis

LIST OF FIGURES

LIST OF TABLES

ABSTRACT

Our work presents a simulation model of human pigmentation disorders. Our model is formed by a set of differential equations that defines a reaction-diffusion system. Our system simulates some features of the human pigmentary system. Changes in this system can lead to imbalances in the distribution of melanin in the skin resulting in artifacts known as pigmented lesions. Our model aims to reproduce these changes and consequently synthesize human pigmented lesions. Our reaction-diffusion system was developed based on biological data regarding human skin, pigmentary system and melanocytes life cycle. The melanocytes are the main cells involved in this type of human skin disorders.

The simulation of such disorders has many applications in dermatology, for example, to assist dermatologists in diagnosis and training related to pigmentation disorders. However, our study focuses on applications related to computer graphics. Thus, we also present a method to transfer the results of our simulation model for textures and images of human skin. In this context, our model contributes to the generation of more realistic skin textures and consequently for the generation of more realistic human models.

Moreover, we also compared the results of our simulation with real pigmented lesions to evaluate the quality of the lesions generated by our model. To perform this comparison we measured some features of real and synthesized pigmented lesions and we compared the results of these measurements. Based on this comparison, we observed that synthesized lesions exhibit the same characteristics of real lesions. Still, for the purpose of visual comparisons, we also present images of real lesions along with images of synthesized lesions. In this visual comparison, we can note that the method used to produce lesions images from the results of our simulation generates images that are indistinguishable from real images.

Keywords: Computer graphics, human skin, melanocyte, melanosome, pigmentary system, pigmentation disorders, pigmented lesions, simulation, skin color, skin simulation.

Simulação de Transtornos de Pigmentação da Pele Humana

RESUMO

Nosso trabalho apresenta um modelo de simulação de transtornos de pigmentação humana. Nosso modelo é formado por um conjunto de equações diferenciais que definem um sistema reação-difusão. Nosso sistema simula algumas características do sistema pigmentar humano. Alterações nesse sistema podem levar a desequilíbrios na distribuição de melanina na pele resultando em artefatos conhecidos como lesões de pigmentação. Nosso modelo tem como objetivo reproduzir essas alterações e assim sintetizar lesões de pigmentação humanas. Nosso sistema reação-difusão foi elaborado tomando como base dados biológicos a respeito da pele humana, do sistema pigmentar e do ciclo de vida dos melanócitos, que são as principais células envolvidas nesse tipo de transtorno.

A simulação desse tipo de transtorno apresenta diversas aplicações em dermatologia como, por exemplo, suporte para o treinamento de dermatologistas e auxílio no diagnóstico de transtornos de pigmentação. No entanto, nosso trabalho se concentra em aplicações relacionadas com computação gráfica. Assim, nós também apresentamos um método para transferir os resultados do nosso modelo de simulação para texturas e imagens de pele humana. Nesse contexto, o nosso modelo contribui para a geração de texturas de pele mais realistas e consequentemente para a geração de modelos de serem humanos mais realistas.

Além disso, nós também comparamos os resultados da nossa simulação com lesões de pigmentações reais objetivando avaliar a qualidade das lesões geradas pelo nosso modelo. Para realizar essa comparação nós extraímos métricas das lesões sintetizadas e das lesões reais e comparamos os valores dessas métricas. Com base nessa comparação, nós observamos que as lesões sintetizadas apresentam as mesmas características das lesões reais. Ainda, para efeito de comparações visuais, nós também apresentamos imagens de lesões reais lado a lado com imagens sintetizadas e podemos observar que o método utilizado para produzir imagens de lesões a partir do resultado do nosso modelo de simulação produz resultados que são indistinguíveis das imagens reais.

Palavras-chave: Computação gráfica, cor da pele, lesões de pigmentação, melanócito, melanossomo, pele humana, simulação, simulação de pele, sistema pigmentar, textura, textura de pele, transtornos de pigmentação.

1 INTRODUCTION

Skin color is determined by several chromophores (BURNS et al., 2010). Melanin, haemoglobin, and carotenoids are the chromophores that contribute significantly to the skin color formation. Among these chromophores, melanin is the most important. Melanin is produced by special skin cells called melanocytes and packed in organelles called melanosomes. The number, size, shape, distribution and degradation of melanosomes vary in different ethnic groups. Furthermore, there are two different types of melanin: eumelanin (black) and phaeomelanin (red). The amount and ratio of eumelanin and phaeomelanin also varies in different ethnic groups. The variations involving the melanosomes and the amount and ratio of the two different melanin types produces the several different human skin color shades.
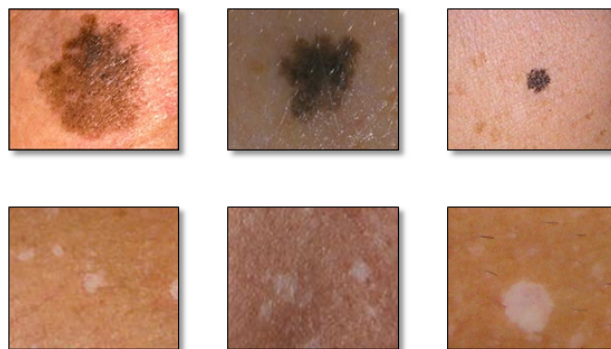
Figure 1.1: Example of real pigmented lesions, in the first row we have hyperpigmented lesions and in the second row we have hypopigmented lesions.

In healthy skin, some regions may show a slight variation in melanin concentration when compared to others regions. Nevertheless, the healthy skin color is usually uniform particularly when evaluated in small regions and disregarding the variations resulting from tanning. Sometimes, the skin may present a non-uniform melanin distribution. This non-uniform distribution can be presented in two different ways. In the first, the melanin concentration increases to levels above normal and this situation is called hypermelanosis. In the second, when the melanin concentration decreases to levels below normal, occurs what it is called hypomelanosis. Hypermelanosis and hypomelanosis are the two types of pigmentation disorders of the human skin. Examples of real hyperpigmented lesions and hypopigmented lesions are shown in Figure 1.1. In Figure 1.1 we can see that hyperpigmented lesions result in dark spots and the hypopigmented lesions result in light spots. The pigmented lesions shown in Figure 1.1 and along this work are from

the dermatological repositories (DERMIS, 2013), (NEW ZEALAND DERMATOLOG-ICAL SOCIETY INCORPORATED, 2013), (SILVA; CALHEIROS, 2013), (USATINE, 2009), (VERROS, 2013), (EASTER et al., 2013) and from our own clinical studies.

Pigmentation disorders are one of the most common disorders associated with the skin. In the United States, this type of skin disorder is observed in 90% of whites older than 60 years and in 20% of whites younger than 35 years (SCHWARTZ; OKULICZ; JOZWIAK, 2012). In Brazil, pigmentation disorders constitute the most common skin disorder in people aged between 40 and 64 years and the second most common in the population aged between 15 and 39 years (SOCIEDADE BRASILEIRA DE DERMA-TOLOGIA, 2006). The simulation of human pigmentation disorders has several applications such as: support dermatologists in the diagnosis and identification of different types of pigmentation disorders; assist in dermatology teaching and training of new dermatologists; and contribute to the synthesis of realistic human skin in computer graphics.

Regarding the diagnosis support, pigmentation disorders simulation is useful since through this simulation is possible to estimate which conditions lead to a specific pigmentation disorder. Thus, by comparing a real lesion image with simulation results we can list possible diagnoses for this disorder based on the conditions that generate results with the same characteristics of the real lesion. In addition, a dermatology student can improve his/her understanding related to human pigmentation disorders by changing these conditions. In other words, through the pigmentation disorders simulation, the dermatology students can become familiar with features of different types of pigmentation disorders. In this sense, we can affirm that the pigmentation disorders simulation also can help in dermatology teaching.

Figure 1.2: A human face model without and with small irregularities, respectively (IGARASHI; NISHINO; NAYAR, 2005).

However, in our work, we focus in applications related to computer graphics which has a long tradition in modeling and rendering of human beings. Thus, the production of realistic human images is one of the goals of computer graphics. Also, we know that real human images are full of irregularities. In this sense, one way to increase the realism of the synthesized human images is through the addition of irregularities in these images. The result of irregularities adding to a human model can be seen in Figure 1.2. We also know that human pigmentation disorders are source of very common and familiar skin irregularities. Thus, the reproduction of human skin pigmentation disorders contributes

to production of more realistic human skin textures in images and in 3D models. Consequently, the reproduction of these disorders contributes to production of more realistic rendering and modeling of human beings.
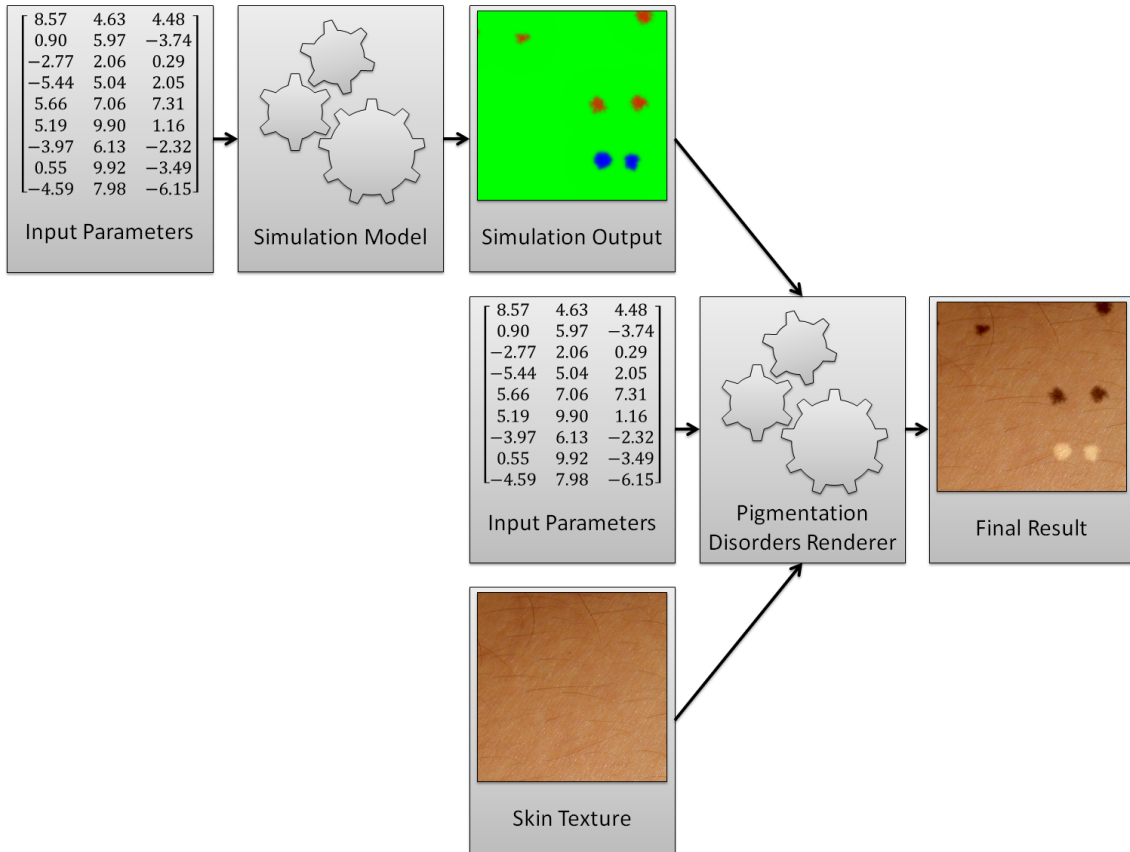
Figure 1.3: Pigmented lesions rendering process. First, a parameters set is used to configure the simulation model. Then, the simulation result and a health skin image are used as input to the renderer. This renderer also is configured with another set of parameters. Finally, with this data, the renderer produces a new image including the pigmentation disorders effects.

A possible solution to reproduce these disorders consists in the composition of multiple skin textures including the effects of these disorders through work of artists. Another solution is to capture the effects of these disorders from real human skin and transfer them to skin textures. In any case, both solutions are expensive because they require either the work of artists or the use of special equipment and subjects with the desired disorders. In our work we use a biologically inspired mathematical model to simulate the human skin pigmentation disorders. Generally, these models are advantageous because they are inexpensive, automated, independent of the ability of artists, and do not require any special equipment.

Our model is described as a set of differential equations that accounts the melanocytes life cycle and the melanosomes production, degradation, and distribution through the skin. In our model, different mutations may occur in the normal melanocytes population. These different mutations unbalance the population of melanocytes and consequently unbalance the production, degradation, and distribution of melanosomes. The main output of our model is the amount of melanosomes in a specific skin region. Then,

this amount of melanosomes is used to generate the visually perceptible effects of the pigmentations disorders in a healthy skin image or texture. These effects consist of hypo-pigmented and hyperpigmented lesions. The rendering of lesions is done by considering a number of attributes of the skin texture or image such as illumination conditions, skin surface geometry, and image scale. In Figure 1.3 we have a brief illustration of the process involved in obtaining our final results. As we can see in Figure 1.3, we use a set of parameters to initialize the simulation model. Most of these parameters have default values. Then, we run the simulation based on these parameters producing an output that is a two-dimensional grid with values that represents the concentration of melanosomes. After that, this concentration is used as input to another module which is responsible for mapping these values to a healthy skin image. This mapping process is also configured by a set of parameters. At the end of this process, an image with a rendered skin lesions is produced. We can see in detail the simulation outputs and the rendering corresponding to these outputs in Figure 1.4.
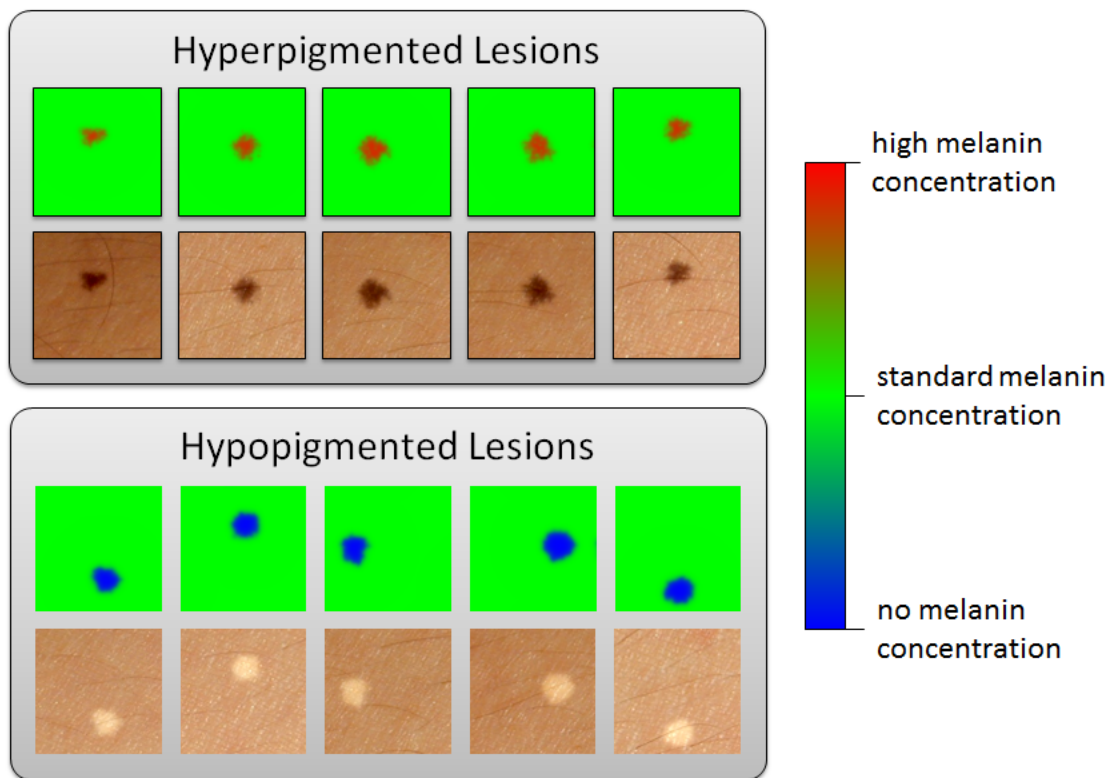
Figure 1.4: Simulation outputs and their corresponding rendering.

1.1 Structure of Our Work

Besides this introductory chapter, in Chapter 2 we discuss the research involving human pigmentation simulation in computer graphics and in dermatology. As we know that human pigmentation disorder is a common feature of human aging process, we also review the computer graphics literature regarding human aging simulation in order to verify if these works include the simulation of human pigmentation disorders. Further, in Chapter 3, we present the biological knowledge regarding the human pigmentation disorders.

Thus, in Chapter 3, we describe the skin structure, function and main cells as well we present the characteristic of the different types human pigmentation disorders simulated by our mathematical model, which we describe in Chapter 4. Also, in Chapter 4, we describe the properties of our model and we validate our model through a comparison with real human pigmented lesions. In the following chapter, we describe the method used to render the simulation model results into healthy skin textures and images. We also show the results of this rendering process in Chapter 5. Finally, in Chapter 6, we summarize our work and describe what can still be explored from it in the future.

2 RELATED WORK

In this chapter we review the research regarding the simulation of human pigmentation disorders. We present research addressing this simulation both in dermatology and in computer graphic context. However, in dermatological context, most work regarding pigmentation disorders using mathematical or computational models deals with automated recognition and diagnosis of pigmentation disorders (STOECKER; LI; MOSS, 1992; LEE, 2001; ALCÓN et al., 2009; EMRE CELEBI et al., 2008; SCHMID-SAUGEONA; GUILLODB; THIRANA, 2003; ZHOU et al., 2010a,b). The use of such models to simulate pigmentation disorders effects is not a much explored topic in dermatology. Nevertheless, the few works regarding pigmentation disorders in dermatological context are reviewed in Section 2.1.

Pigmentation disorders are most commonly found in people of advanced age. In this sense, we can consider pigmentation disorders as a common feature of human aging process and, because of this, we also review the works reproducing human aging effects in computer graphics. These works are presented in Section 2.3.

However, before we review the works regarding the human aging in computer graphics, we list the main changes that the human body suffers as it ages. We list these changes aiming to provide background information regarding human aging. We just list the visual changes of human aging process because these changes are relevant in computer graphics context. These changes are presented in Section 2.2.

Also, we classify and analyze the works from computer graphics on human aging in Section 2.4. Then, we review only the works from computer graphics which include the reproduction of any type of pigmentation disorder in Section 2.5.

2.1 Pigmentation Disorders Simulation in Dermatology

In dermatology, the simulation of pigmentation disorders usually focuses on the reproduction of the light interactions with the pigmented lesion. There are two main approaches for simulation of these light interactions.

First, this simulation can be done by using computer models. In the work by Patwardhan, Dhawan, and Relue (PATWARDHAN; DHAWAN; RELUE, 2005), the light interactions with the skin lesions are simulated through Monte Carlo techniques.

The other approach for this type of simulation is done by using chemical pigmented skin simulants. These simulants try to reproduce the absorption and diffusion of light in the normal skin and in the pigmented skin lesions. In the work by Lualdi et al. (LUALDI et al., 2002), the simulant is formed by a transparent silicone rubber with Al_2O_3 particles, melanin, and different types of cosmetic powders. However, these simulants can be made by different compositions. For example, Mazzoli, Munaretto, and Scalise (MAZZOLI;

MUNARETTO; SCALISE, 2008) use a transparent polyvinyl alcohol hydrogel with appropriate amounts of optical scatterers and Liquid India ink to simulate the melanin and all the other skin chromophores.
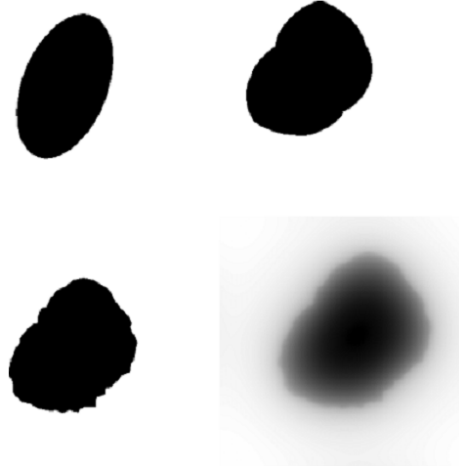
Figure 2.1: Lesion shape simulation steps by She et al. (SHE et al., 2006).

In our work we do not focus on the light interactions with the pigmented lesions. Our objective is to reproduce the pigmented lesions characteristics found in clinical images. A work with this same objective was realized by She et al. (SHE et al., 2006).

The work by She et al. (SHE et al., 2006) synthesize a skin lesion with known characteristics including shape, color, and skin pattern. They do not try to transfer a synthesized skin lesion to an existing skin image. Thus, they have to simulate all the artifacts present in a real clinical skin lesion image such as skin pattern, hair, and specular reflection. In our approach, we maintain the artifacts present from the skin image where the lesion will be transferred.
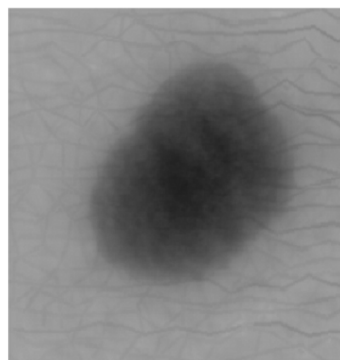
Figure 2.2: Final result by She et al. (SHE et al., 2006).

The work by She et al. (SHE et al., 2006) simply tries to reproduce the visual characteristics of a skin lesion. Thus, it does not use a biological inspired method to generate the lesion shape. For this, it applies a simple random modifications to an ellipse which was also produced randomly. Then, a 2D first-order low-pass filter is applied to smooth the border of the modified ellipse image. Figure 2.1 illustrates this process. Differently

from our approach, which is based on the pigmentary system dynamics, this work cannot simulate the evolution of a skin lesion shape over time.

The others characteristics and artifacts of the skin and of the lesion are generated through different techniques. Skin pattern is simulated with segmented lines with variations in length, orientation and intensity. Skin and lesion textures are modeled by an auto-regressive process. The skin lesion color is generated by mixing skin and lesion textures. Finally, an inflammation area and image artifacts such as hair and specular reflection may be added. Figure 2.2 shows an example of final result by this work.

The work by Dhawan and Sim (DHAWAN; SIM, 1992) also generate skin lesions but with a different purpose from our work. This work aims to evaluate a skin lesions segmentation algorithm. Thus, it generates a skin lesion simply by overlapping ellipses with different sizes and textures. This approach generates very unrealistic results as we can see in Figure 2.3.
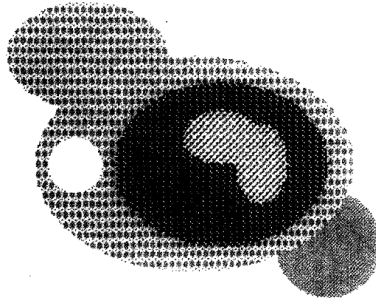
Figure 2.3: Result by Dhawan and Sim (DHAWAN; SIM, 1992).

2.2 Human Appearance Changes Due To Aging

The aging process is the source of several changes in the appearance of our bone structure, musculature, skin and other body parts. In this section, these changes are grouped according to the specific parts of the human anatomy and organs where they occur. First, we describe the main changes occurring in the body as a whole. Then we describe the changes related to the skin in general. Finally we detail the changes that occur in specific parts of the body such as neck, face, hair, etc. The information presented in this section was compiled mainly from (WHITBOURNE, 2007) and (ALBERT; RICANEK JR; PATTERSON, 2007).

2.2.1 Body

The bones constantly rebuild themselves and the old cells that constitute them are destroyed and replaced by new cells. However, as we age, we lose bone mass because the rate of bone destruction increases compared to the renewal rate. This bone mass reduction makes our spine becomes shorter. Consequently, we become shorter because of this loss of bone mass in the spine. Thus, one of the changes that occur in our bodies as we age is a decrease in our height.

Our weight also changes as we age. Our weight increases from 20s until the mid-50s and declines after that. Our body mass index (BMI) increases through the years of middle adulthood by the accumulation of body fat around the waist and hips. The weight

loss occurring thereafter is not related to the loss of this accumulated body fat. Older adults lose weight due primarily to a reduction of fat-free mass (FFM). The FFM reduces because muscle fibers decrease in size and number. The bone mass loss mentioned above also contributes to this weight reduction.

In short, we lose bone mass and muscle and accumulate fat and this makes our height decrease and the shape of our bodies and our weight change.

2.2.2 Skin

The skin starts to wrinkle as early as the 20s and 30s. However, this change in the skin is most visible in older people. Over the years, the wrinkles in the skin become increasingly deep and visible. By the 70s and beyond, grooves, creases, and lines on the skin are overdone.

Over time, not only the skin wrinkles are intensified. The loss of skin elasticity is also accentuated. In very old people this loss of skin elasticity causes the skin to become unable to return to its original state after being stretched.

The skin has an inner layer of subcutaneous fat. This layer gives to the skin its opacity and smooth curves in the legs, arms, and face. The subcutaneous fat layer start to thin in the middle of adulthood and continues to thin over the years. This thinning of the subcutaneous fat layer causes the skin to become more and more translucent and the veins and bones underneath become visible. As this layer thins, it provides less support for the upper layers. Consequently, the skin becomes saggy.

In addition to these changes, the skin also presents the following alterations:

- A yellowish discoloration (OHSHIMA et al., 2009).

- The development of age spots which are small discrete macules with irregular borders scattered through a skin region, usually a sun-exposed region such as the face, hands, and arms. The age spots size vary from 1cm to 3cm but can reach up to 5cm and their color vary from light brown to dark brown.

- The development of pigmented outgrowths known as moles.

- The appearance of large irregularities in the blood vessels known as varicose veins on the skin of the legs.

- Capillaries and arteries in the skin may become dilated and more visible.

2.2.3 Neck

Basically, the visible changes presented by the neck as we age are consequences of skin changes. However, as the neck skin is thin compared to the skin in other body regions, the changes in the neck skin are more pronounced. In this way, in the 50s, wrinkles in the neck skin start to appear. In the 60s, the soft tissues in the neck lose its firmness and then they sag. Just like the skin on the other body regions, by the 70s and beyond, the lines, grooves, and the creases in the neck skin are all exaggerated.

2.2.4 Nails

The nails are also part of the skin, and even as the skin, they change as we age. Thus, similarly to the skin, the nails also acquire a yellowish hue over the years. The toenails may to develop ridges and thickened areas. The toenails may also bend enough to become similar to hooks.

2.2.5 Teeth

The teeth show a discoloration due to loss of their enamel surface and staining from coffee, tea, food and tobacco. Tooth loss may also occur. However, due to the constant improvements in dental hygiene, the tooth loss tends to decrease over the generations.

2.2.6 Face

Most of the face age changes are consequences of the bone alterations in the cranium and of the facial soft tissues sagging over the years. These changes cause significant alterations in the face appearance. Thus, as we get old, the face contour, the face edges and the size and position of nose, lips, and ears change due to the alterations in the skull bones and in the facial soft tissues.

Regarding the bone alterations, the cranium increases in size horizontally over the entire adult lifetime. The face height also tends to increase with age due to craniofacial skeleton alterations over the years. There is an increase in the mandibular length as we age. Further, in females, the mandibular arch increases, and the mandible rotates. In the males, the maxillary and mandibular arches increase. The maxillary retrusion is another feature of aging. Retrusion is a backward displacement and the maxillary retrusion contributes to the formation of the diagonal wrinkle from the base of the either side of the nose to the outer edge of the mouth. Besides the maxillary retrusion, the other changes in the maxillary and mandible affect the position of the nose and chin, and make the lips seem more retrusive. When tooth loss occurs, the remodeling in the maxillary and in the mandible may result in a concave appearance to the face, a hollow look to the cheeks, and a decreasing in the jaws.

Concerning the facial soft tissues, their age changes start in the 20s. Several lines, grooves, and creases arise in the face in the 20s and in the subsequent years. These lines, grooves, and creases become increasingly apparent in the years after their arising. The lines, grooves, and creases that appear on the face with aging are listed in Table 2.1 according to the decade in which they appear. By the 50s and beyond, creases, grooves, and lines become more prominent to the point that they present themselves quite exaggerated.

In the 20s:	Horizontal lines across the forehead.
	Vertical lines between the eyebrows.
	Faint lines around the outer corners of the eyes popularly known as "crow's feet".
In the 30s:	Horizontal lines at the top of the nose between the eyes.
	Lines from the outer corners of the base of the nose diagonally down to the sides of the mouth.
In the 40s:	Crease below the inner corner of the eyes down diagonally and laterally over the cheeks.
	Lines around the mouth.
	Horizontal lines at each corner of the mouth extending the mouth width.
	Horizontal groove below the mouth and above the chin.

Table 2.1: The decades in which specific facial lines, grooves and creases appear.

Also with respect to the facial soft tissues, the following changes occur as we age:

- The eyebrows may drop.

- The upper eyelid may drop.

- The areas around the eyes become baggy due to the accumulation of fat, fluid and dark pigmentation.

- The lower jaw become less firm.

- The lips may become thin.

The overall face appearance is also affected by the changes in the appearance in the nose, ears, lips and hair. These changes are described in the following sections.

2.2.6.1 Nose

Changes in the cartilage of the nose cause it to increase in size as we age. More specifically, the size and length of the nose increase. Furthermore, the nose moves forward and downward over the years.

2.2.6.2 Ears

Similarly as in the nose, the changes in the cartilage of the ears cause them to continue increasing their dimensions over the years. The ears in males are larger and longer when compared to females of the same age. On the other hand, the earlobe height and width are similar in both sexes. The increase in ear height as we age occurs mainly due to the increase in earlobe height. The earlobe width decreases considerably as we get older.

2.2.6.3 Lips

The most noticeable changes in the lips shape occur between 15 and 20 years of age in the women, and between 15 and 25 years of age in the men. For both sexes, from 21 to 26 years of age the upper lip height increases substantially, the lip thickness reduces, the distance between the upper lip and the nose increases, and the distance between the lower lip and the chin also increases. Still for both sexes, between ages 15 and 25 years the lips retract and this tends to continue between ages 25 and 45 years. Furthermore, in the 30s and 40s, the lips move downward, flatten, and lengthen. Usually, age related changes in the lips arise earlier in females than in males. This happens because the females often show earlier growth, maturation, and senescence relative to males.

2.2.7 Hair

As we get older our hair becomes gray and sooner or later turns white due to the loss of pigmentation. The different shades of gray in one's hair color are the result of the combination of the unpigmented hairs with the remaining pigmented hairs. The rate at which the hair changes its color varies greatly from person to person. The hair also becomes thinner and, due to the destruction of germination centers in the hair follicles, the amount of hair decreases over the time. This form of hair loss affects 95% of adult men and 20% of adult women. In this form of hair loss, the hair follicles stop the production of the normal hair, which is long, thick, and pigmented. Instead of the normal hair, the hair follicles start to produce a short, fine, unpigmented and largely invisible hair named vellus hair. Eventually, even that hair is not visible because it no longer protrudes from the follicle. While the hair stops growing on the top of the head, it may appear in places such as the ears, the chin on women, and around the eyebrows.

2.3 Human Aging in Computer Graphics

In this section we review research addressing human aging effects simulation in computer graphics. Most of these works are restricted to faces and address the more conspicuous visual effects, such as wrinkles, and face shape variation. We can broadly classify these works in either 2D or 3D approaches.

2.3.1 2D Approaches

Hussein (HUSSEIN, 2002) proposed two approaches towards modeling the facial aging. Each of these approaches addresses a different aging effect in the face. One of these effects is the facial shape changes due to aging. To address this effect, the facial shape is deformed based on a model developed according to the face anthropometry theory. This theory provides a rich description of the face geometry and its changes over the years. The set of lines, grooves and creases that arises in the face with the aging, from now on simply treated as facial wrinkles, is the other addressed effect. The simulation of the facial wrinkles uses a model elaborated based on what is called the bidirectional reflectance distribution function (BRDF) quotient image technique. The Figure 2.4 shows the results of the work of Hussein (HUSSEIN, 2002).

Figure 2.4: Facial aging results of Hussein (HUSSEIN, 2002) by combining wrinkle simulation and facial deformation.

Ramanathan and Chellappa (RAMANATHAN; CHELLAPPA, 2008) also proposed two approaches to reproduce the facial wrinkles and the facial shape changes due to aging. The facial shape changes are reproduced by a physically-based parametric muscle model. This model accounts for the physical properties and geometric orientations of the individual facial muscles. To reproduce the facial wrinkles they alter the gradient of the image where the wrinkles will be applied based on one of the patterns of wrinkles learnt from a set of training images. The results of the work of Ramanathan and Chellapa are shown in Figure 2.5.

Figure 2.5: The results of Ramanathan and Chellappa (RAMANATHAN; CHELLAPPA, 2008). The first column shows the original images where the aging effects will be applied. The second and third columns show the result of the facial shape transformation with two different wrinkles patterns.

The work of Hussein (HUSSEIN, 2002) just requires one source image. The work of Ramanathan and Chellappa (RAMANATHAN; CHELLAPPA, 2008) also needs no additional images to reproduce the facial shape deformations. However, the approach to generate the facial wrinkles in this work requires a database of old people images for the production of the wrinkles patterns that are transferred to the images where the aging simulation will be applied.

As in this approach, all the works presented below in this section require a set of people images in order to reproduce the aging effects in a specific input image. Basically, the aging features are transferred from one or several images in this set to the image where the aging effects will be applied through some specific technique.

In the work of Kasai and Morishima (KASAI; MORISHIMA, 2009), the aging features of the facial shape and facial texture are modeled based on the analysis of real human face database. These aging features are obtained by averaging and filtering a 600 face database with 3D range scan data and frontal texture with age and gender information. Thus, it is possible to make a character younger or older by blending the original character face texture with the aging features obtained from this database. It is mentioned that face aging features like age spots are reproduced in this aging approach. However, no age spot was seen in the presented results.

The work of Liu, Zhang, and Shan (LIU; ZHANG; SHAN, 2004) proposed a method to transfer, in images, the geometric details from a surface to another. These geometric details are captured from a single image independently of the surface reflectance properties. Then, these captured geometric details can be transferred to another surface producing a new surface with the captured geometric details and preserving its reflectance properties. One of the applications of this method is to simulate the aging process through the transfer of the geometric details from the skin of an old person to a young person. Thus, this

method was used to add wrinkles and moles in a young face image making it look old, as we can see in Figure 2.6. This method can be used to add wrinkles, age spots and moles not only to the face but also to other body parts.

Figure 2.6: The results of Liu, Zhang, and Shan. (LIU; ZHANG; SHAN, 2004). From left to right: the original face image, the simulated face with fine details transferred, and the simulated face image with coarse details transferred.

The work of Hubball, Chen, and Grant (HUBBALL; CHEN; GRANT, 2008) uses a data-driven framework for automatic aging facial transformations. This work proposed a parameterized model to encode the aging transformation in addition with a traditional model to describe the face. An evolutionary computing approach was used to learn the relations between these two models. In short, based on a database of face images in different ages, the shape of a specific face image is transformed to seem old or young. This work addresses only the facial shape changes due to aging and do not deal with wrinkles or other skin texture changes arising from the aging process. Figure 2.7 shows the results of this work.

Figure 2.7: The results of Hubball, Chen, and Grant. (HUBBALL; CHEN; GRANT, 2008). The first column shows the original images where the aging effects will be applied. The second column shows the result of the facial aging transformation.

In the work of Suo et al. (SUO et al., 2010) the face is broken down into its main constitutive parts (mouth, nose, eyes, etc.) and represented as a hierarchical graph. Aging in this graph is represented as a Markov chain which provides variability and aging models among age groups. The parameters used in this work are learned from a large face data set. The authors claim to address facial shape changes, facial wrinkles, and pigmentation disorders. However, the results do not include any pigmentation disorder. Figure 2.8 illustrates the results of this work.
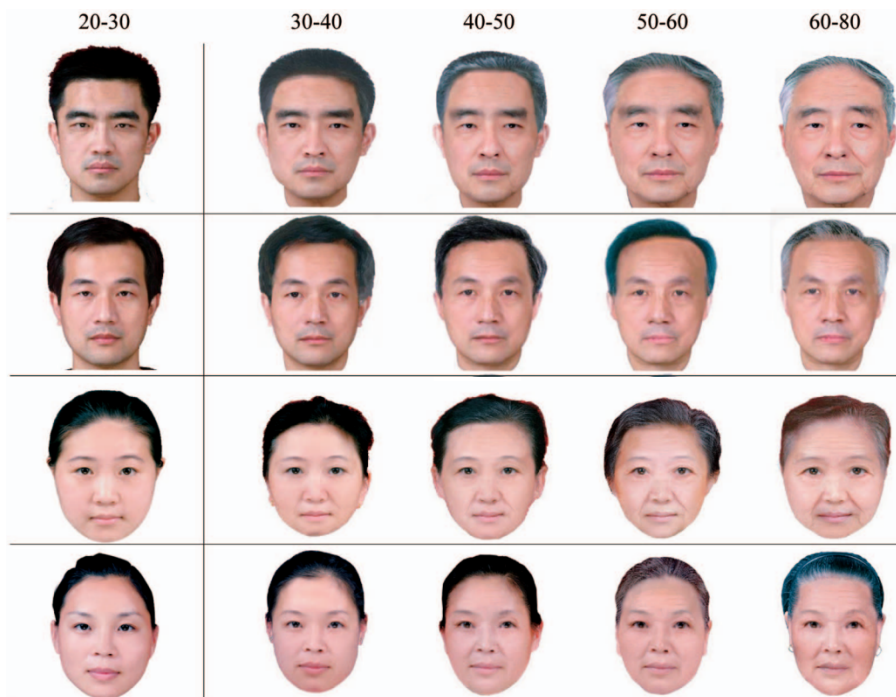
Figure 2.8: The results of Suo et al. (SUO et al., 2010). The first column is the original images of the individuals. The second to fifth columns are synthetic aged images at four consecutive age groups.

The work by Tiddeman, Stirrat and Perrett (TIDDEMAN; STIRRAT; PERRETT, 2005) addresses aging as a transformation process between two groups of images: images of young people, and images of old people. The proposed technique transforms the low resolution image data using the mean differences between the two groups. However, this technique converges on more specific texture features at the finer resolutions. The high and low resolution information are separated by transforming the image into a wavelet domain. For each point, a mapping from the original group to the target group is calculated based on the probability distributions of the wavelet values. These distributions are obtained from sample images. The proposed technique allows not only aging transformations but also gender transformations, from female to male, for example.

The work by Gandhi (GANDHI, 2004) produces signature images, or age prototypes, for various age groups from a database created with face images collected from the Internet. These images range in age from 15 years to 99 years. The aging simulation consists in transfer the data from an age prototype to a specified input image. This work deals only with simulation of the facial wrinkles. Figure 2.9 shows some results of this work.

(a) Target Age: 50 years   (b) Target Age: 60 years   (c) Target Age: 70 years   (d) Target Age: 80 years
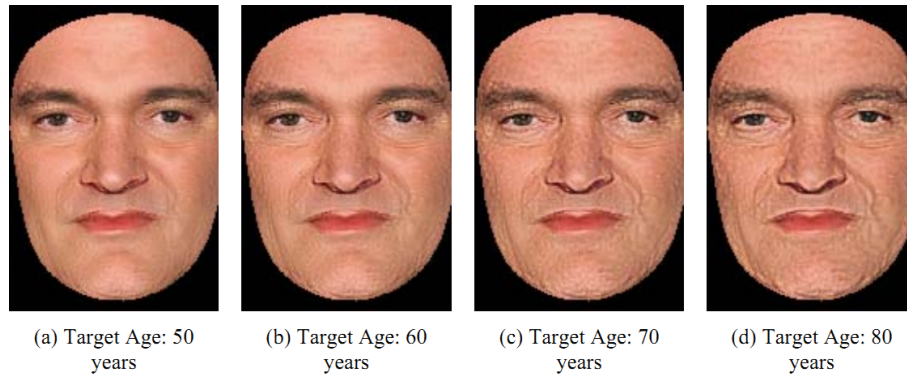
Figure 2.9: Aging progression simulation by Gandhi (GANDHI, 2004). A aging progression to 50, 60, 70 and 80 years respectively.

2.3.2 3D Approaches

The work of Tost (TOST, 2005) uses a bump maps to reproduce the wrinkles, a jitter-texture technique to generate the age spots which are blended in the skin texture using different alpha-values. This work also simulates the skin color change due to aging. Figure 2.10 shows the result of this work. Although Figure 2.10 shows an aging face, this work aims to reproduce the general skin appearance and not only facial skin aging. Thus, this paper presents an approach to render the skin from different body parts in different aging levels.

Figure 2.10: An aging process simulation sample by Tost (TOST, 2005). On the left we have the young face model, and, on the right, the same face model with added aging features.

The work by Scherbaum et al. (SCHERBAUM et al., 2007) represents the 3D face geometry as a morphable model and assumes that this geometry follows curved trajectories in face space as it gets old. These trajectories are computed based on a non-linear function which is learned from a database of 3D face scans of teenagers and adults. This work applies the aging transformation through the following process: first, the 3D face model from the input image is reconstructed; after that, the aging transformations are applied in this model; and finally, the model is rendered back into the input image or into another image of the same individual. This work reproduces the facial shape and texture alterations due to aging and focuses on the aging from a child face to a teenager or adult face. None of the results in this work shows an aging transformation that results in an aged face appearing 40 years or older. Some results of this work are shown in Figure 2.11.
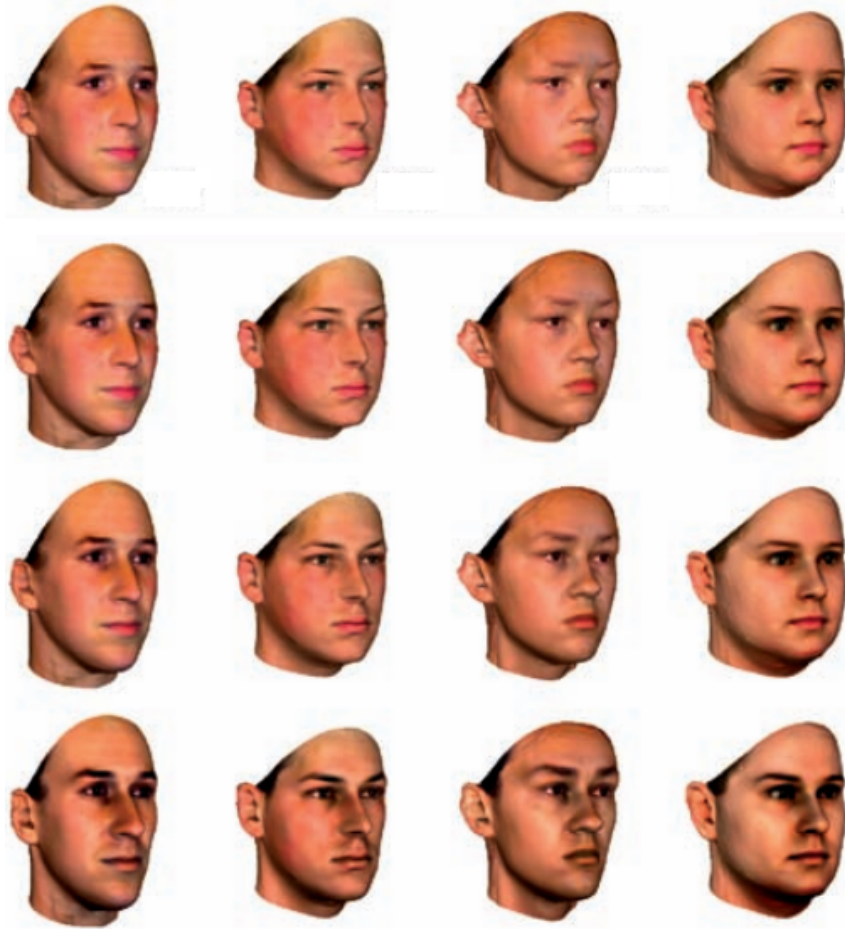
Figure 2.11: The results of Scherbaum et al. (SCHERBAUM et al., 2007). The first row shows 3D face models obtained by through laser scans of real human faces. The next rows show these face models aged 180, 240 and 360 months respectively.

In the work by Si, Kong and Yin (SI; KONG; YIN, 2009) the color gabor wavelet transform is used to extract the aging features from a 3D face texture. Then, these features are transferred to another 3D face texture through wavelet reconstruction.

The work by Golovinskiy et al. (GOLOVINSKIY et al., 2006) uses a statistical technique to analyze and synthesize small three-dimensional facial features, such as wrinkles and pores. In this work, the geometry of several faces was acquired in high-resolution from people across a wide range of ages. For each acquired face geometry, the skin surface details were separated from a smooth base mesh using displaced subdivision surfaces. The resulting displacement maps were analyzed in a framework adapted to identify statistics that vary over the face surface. After that, the identified statistics are used to generate convincing details on arbitrary face meshes. The result of this work is shown in Figure 2.12.

A method to reproduce the facial aging based on artistic techniques is proposed in the work of Uchiyama et al. (UCHIYAMA et al., 2007). More specifically, in this work, the visual aging simulation of a 3D face model is achieved by applying an artistically-based method which was developed considering expression techniques used by artists in their work. Figure 2.13 illustrates the result of this artistically-based method for the visual simulation of facial aging.

(a) Original low-resolution face   (b) Synthesized detail   (c) Aged
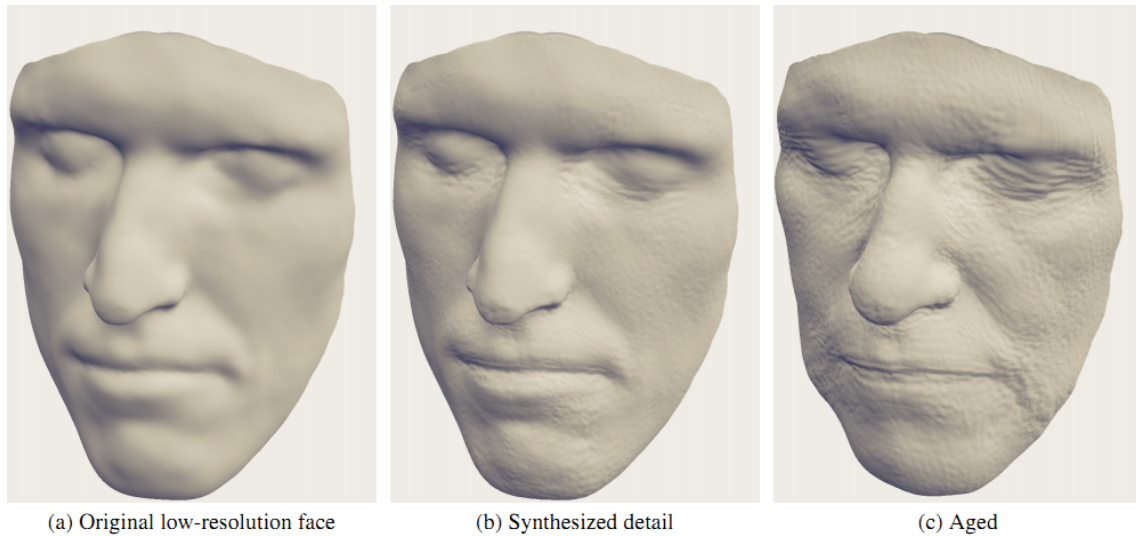
Figure 2.12: A sample result of Golovinskiy et al. (GOLOVINSKIY et al., 2006). Geometric details are synthesized in the low-resolution face mesh. Then, this face mesh is aged by the adjustment of statistics to match those of an old person.

Boissieux et al. (BOISSIEUX et al., 2000) propose two approaches to simulate the facial wrinkles in their work. The first approach uses generic masks of pre-computed wrinkles to change the luminance and coloration of the 3D face model texture bringing about the wrinkles and other aging artifacts. In the second approach, the 3D face model is deformed by geometric or physically based techniques. The results of this approach are generated by the computation of the deformation of the geometry and structure of the skin. In this approach, the skin is modeled as a volumetric substance with layers of different materials and a finite element method is used to compute the deformations in this skin model.

Figure 2.13: The facial aging of Uchiyama et al. (UCHIYAMA et al., 2007). A young face model, on the left, and this same model aged, on the right.

Also regarding facial wrinkles simulations, the work of Wu, Magnenat Thalmann, and

Thalmann. (WU; MAGNENAT THALMANN; THALMANN, 1994) proposes a simple plastic-visco-elastic model which allows simulation of facial wrinkles. In Wu et al. (WU et al., 1999) the facial simulation is split into facial surface deformation and wrinkles generation. The facial surface deformation is based on three-layered facial structure (muscle, connective tissue, skin) and the layer that represents the facial muscles provides the forces to deform the skin layer while the connective tissue layer constrains the skin movement. The wrinkles generation uses a synthetic texture and the wrinkles are dynamically produced by a linear plastic model. Figure 2.14 show the results of this work.

Figure 2.14: A result of Wu et al. (WU et al., 1999) that shows a sequence of facial aging process along with facial expressions.

Still with respect to the facial wrinkles simulation, in Wu, Kalra and Magnenat Thalmann (WU; KALRA; THALMANN, 1997), the facial wrinkles simulation is computed based on a biomechanical model which considers the skin as a membrane that suffers large deformations. The skin textures are produced by combining micro and macro structural skin patterns with real skin images. Another proposal for the facial wrinkles simulations is described by Wu, Beylot and Thalmann (WU; BEYLOT; MAGNENAT THALMANN, 1999). In this work, muscle patches are automatically adapted to the individuals faces, the connective tissues ate simulated as simple springs, and the facial deformations and wrinkles generation are estimated based on a elaborated biomechanical model.

2.4 Classification and Analysis of Works on Human Aging in Computer Graphics

We have listed the visual changes related to the human aging process in Section 2.2 and analyzed the research in computer graphics that aims to simulate these visual changes in Section 2.3. Table 2.2 summarizes these changes and the works in computer graphics that deal with them. The first column of this table lists the visual effects of human aging and the second lists the works that aim to reproduce a specific effect. The Facial Wrinkling effect covers all the grooves, creases, and lines that arise in the facial skin as described in Section 2.2. Similarly, the Skin Wrinkling effect covers all the grooves, creases and lines that arise in the skin all over the body. The Skin Texture Changes effect includes the yellowish discoloration and the opacity alteration of the skin in general. The Facial Texture Changes effect includes the same changes of the Skin Texture Changes effect but restricted to the face. The Facial Shape Changes effect involves all the geometric alterations in the face together with the alterations in the position and shape of the nose and lips.

As we can see in Table 2.2, the human aging simulation is a much explored topic in computer graphics. However, still there are many visual aging effects not covered by the works in computer graphics. The most part of the evaluated works focuses only in the facial wrinkles or facial shape changes but, as described in Section 2.2, the aging changes affect the entire human body appearance. All the visual changes involving the body shape due to the bone mass loss, muscle mass loss, and fat accumulation are ignored. Furthermore, in the evaluated works, there is no mentions related the simulation of the specifics changes involving the teeth, ears, nails, and neck. Also, the alterations involving the irregularities in the blood vessels and the appearing of these irregularities in the skin are no mentioned in the evaluated works. The works by Kasai and Morishima (KASAI; MORISHIMA, 2009), Suo et al. (SUO et al., 2010), and Tost (TOST, 2005) mention to address the age spots. However, the age spots are observed only in the results of the work by Tost (TOST, 2005). Further, this work shows very unrealistic age spots since all these age spots present a perfect circular shape and a uniform color and these features are not observed in the real age spots. The work of Si, Kong and Yin (SI; KONG; YIN, 2009) mention to address the effect but this work does not present any sample results, thus the results of this work could not be evaluated.

Table 2.3 classifies the evaluated works according to the type of approach used for reproduction of the human appearance changes due to aging process. The Real Data Dependent approachs require the capture of real data from old people, through images or 3D scans, and use some specific method to isolate and transfer the aging features from the images or models of old people to the images or models of young people. The Model-Based approachs use computational models to reproduce the aging features through the evaluation of geometric, chemical or physical properties involved in the process in which these aging features are generated.

In Table 2.3 we can observe that there are few works that do not requires the capture of real data from people to reproduce the aging effects. These data-driven approaches are strongly depending of the quality of their data and to create a database with good quality images from peoples in different ages, genders and ethnic groups is a very difficult task. Thus, we can observe that there is the opportunity to the production of computational models to simulate the visual effects of the aging process. Still regarding the information available in Table 2.3, we can observe that the work by Tost (TOST, 2005) uses two dif-

Visual Effect Of Human Aging	Works Addressing The Effect
Age Spots Appearing	(KASAI; MORISHIMA, 2009) (SUO et al., 2010) (TOST, 2005)
Facial Shape Changes	(GOLOVINSKIY et al., 2006) (HUBBALL; CHEN; GRANT, 2008) (HUSSEIN, 2002) (KASAI; MORISHIMA, 2009) (RAMANATHAN; CHELLAPPA, 2008) (SCHERBAUM et al., 2007) (SUO et al., 2010) (TIDDEMAN; STIRRAT; PERRETT, 2005) (UCHIYAMA et al., 2007)
Facial Texture Changes	(HUSSEIN, 2002) (KASAI; MORISHIMA, 2009) (SCHERBAUM et al., 2007) (SUO et al., 2010) (TIDDEMAN; STIRRAT; PERRETT, 2005) (TOST, 2005)
Facial Wrinkling	(BOISSIEUX et al., 2000) (GANDHI, 2004) (GOLOVINSKIY et al., 2006) (HUSSEIN, 2002) (KASAI; MORISHIMA, 2009) (LIU; ZHANG; SHAN, 2004) (RAMANATHAN; CHELLAPPA, 2008) (SI; KONG; YIN, 2009) (SUO et al., 2010) (TIDDEMAN; STIRRAT; PERRETT, 2005) (TOST, 2005) (WU; MAGNENAT THALMANN; THALMANN, 1994) (WU; KALRA; THALMANN, 1997) (WU et al., 1999) (WU; BEYLOT; MAGNENAT THALMANN, 1999)
Hair Loss	(HUSSEIN, 2002) (SUO et al., 2010)
Hair Pigmentation Loss	(SUO et al., 2010)
Hair Thinning	(SUO et al., 2010)
Moles Arising	(LIU; ZHANG; SHAN, 2004)
Skin Wrinkling	(LIU; ZHANG; SHAN, 2004) (TOST, 2005)
Skin Texture Changes	(TOST, 2005)

Table 2.2: The visual effects of human aging addressed in computer graphics.

Work	2D or 3D?	Used Approach	Focused Body Area
(BOISSIEUX et al., 2000)	3D	Model-Based/Real Data Dependent	Face
(GANDHI, 2004)	2D	Real Data Dependent	Face
(GOLOVINSKIY et al., 2006)	3D	Real Data Dependent	Face
(HUBBALL; CHEN; GRANT, 2008)	2D	Real Data Dependent	Face
(HUSSEIN, 2002)	2D	Model-Based	Face/Hair
(KASAI; MORISHIMA, 2009)	2D	Real Data Dependent	Face
(LIU; ZHANG; SHAN, 2004)	2D	Real Data Dependent	Skin
(RAMANATHAN; CHELLAPPA, 2008)	2D	Model-Based/Real Data Dependent	Face
(SCHERBAUM et al., 2007)	3D	Real Data Dependent	Face
(SI; KONG; YIN, 2009)	3D	Real Data Dependent	Face
(SUO et al., 2010)	2D	Real Data Dependent	Face/Hair
(TIDDEMAN; STIRRAT; PERRETT, 2005)	2D	Real Data Dependent	Face
(TOST, 2005)	3D	Data Dependent/Model-Based	Skin
(UCHIYAMA et al., 2007)	3D	Artistically-Based	Face
(WU; MAGNENAT THALMANN; THALMANN, 1994)	3D	Model-Based	Face
(WU; KALRA; THALMANN, 1997)	3D	Model-Based	Face
(WU et al., 1999)	3D	Model-Based	Face
(WU; BEYLOT; MAGNENAT THALMANN, 1999)	3D	Model-Based	Face

Table 2.3: The approaches used to the visual reproduction of the human aging.

ferent approaches to address the visual effects of the human aging. This work requires two or more bump maps to reproduce the skin wrinkles. However, there is no mention to the way how these bump maps are acquired and this justifies the use of the term Data Dependent in the row of the Table 2.3 related to this work. Besides this data dependent approach, this work also presents a simple random computational model to generate the age spots. The works by Boissieux et al. (BOISSIEUX et al., 2000), and Ramanathan and Chellappa (RAMANATHAN; CHELLAPPA, 2008) also combine two different approaches in order to reproduce the changes in the human appearance due to aging process. According to the information in Table 2.2 and in Table 2.3, we can observe that there are few works in 3D that reproduce the aging effects other than the facial wrinkling. Thus, there is an opening for conducting research in 3D computer graphics dealing with other aging effects other than facial wrinkling.

From the survey of human visual changes due to aging in Section 2.2, and from the analysis of the works in computer graphics addressing this changes in Section 2.3, we can see that the human aging simulation is a relevant topic in computer graphics but still open. Furthermore, we just focus on the aging changes that can be perceived in a non-animated character model or image. But, the aging process also affects the human mobility (WHITBOURNE, 2007), for example. Thus, it is also possible to explore in computer graphics the way how the aging process affects the animation of a human character.

2.5 Pigmentation Disorders in Computer Graphics

Age spots are the only pigmentation disorder addressed in the works listed in Section 2.3. As can be seen in Table 2.2, the only works which deals with age spots are (KASAI; MORISHIMA, 2009), (SUO et al., 2010), and (TOST, 2005).

The works by (KASAI; MORISHIMA, 2009) and (SUO et al., 2010) use an approach based on databases. That is, both works do not simulate age spots, they only transfer the age spots captured and saved in database to another image. This type of approach is strongly dependent on the database quality. A disadvantage of approaches based on database is that transferred age spots can be visually inconsistent with the skin color in the region where the spots were applied. For example, a age spot from a light skin subject applied in an image from a dark skin subject will not generate a natural result.

(TOST, 2005) uses a simple technique called jitter-texture to generate age spots. In this technique, a texture is divided in grids. In random grid elements a round spot is drawn with a random position and random size. The spots are drawn with different transparency levels and blended in the skin texture. We can see the result of this work in Figure 2.10. Obviously, this work ignores some real characteristics of age spots. For example, these spots are not always rounded. In addition, blending a spot with a skin texture simply using different transparency levels do not generates visually consistent results.

None of the techniques used by (KASAI; MORISHIMA, 2009), (SUO et al., 2010), and (TOST, 2005) regarding age spots have a biological basis. These techniques simply attempt to reproduce age spots in skin images without age spots. Also, differently from our approach, as can be seen in Table 2.3, these works focus only on the human face skin. Moreover, although these works claim to reproduce human age spots in their results, just the work by (TOST, 2005) presents results showing age spots.

2.6   Summary

In this chapter, we reviewed the works that aim to simulate or reproduce the pigmentation disorders in dermatological and computer graphics context. Based on the information in this chapter we can note that there are few works regarding the simulation of pigmentation disorders by using computer models in both contexts. In dermatological context, most work regarding pigmentation disorders focuses on automated diagnosis support or in the simulation of the light absorption and diffusion in a pigmented lesion. In computer graphics context, the works reproducing the visual effects of pigmentation disorders do not focus directly on the pigmentation disorder but on the generic simulation of human aging effects. Thus, we can note that the topic addressed in our work is not a much explored research topic both in dermatology and in computer graphics.

3 BIOLOGICAL BACKGROUND

Humans are very aware and sensitive to the skin appearance. Skin is the most visible human body tissue. The skin presents an area around 2 m^2 and this makes it the largest human organ in terms of surface area. Also, skin is the largest human organ in terms of weight representing in adults around 8% of the total body weight. Skin has a very complex structure and performs several important functions in human body. This structure is explained in Section 3.2 and the main skin functions are detailed in Section 3.1. Furthermore, in this chapter, we explore the biological aspects regarding the human skin. We focus on relevant aspects to understanding human pigmentation disorders. Thus, we also explain the cells characteristics related to the pigmentary system in Section 3.3. Later in Section 3.4, we present the different types of pigmentation disorders explored by our work. The information presented in this chapter was compiled from (BURNS et al., 2010) and (IGARASHI; NISHINO; NAYAR, 2005).

3.1 Skin Functions

Human skin has several functions and the most obvious one is to establish a protective barrier isolating the human body of the surrounding environment. In this sense, the skin prevents the outward passage of important substances to the maintenance of our body, prevents the inward passage of dangerous chemicals and microorganisms, and absorbs the ultraviolet radiation from the sun.

The skin superficial layer is impermeable and works as a physical barrier avoiding water loss. The skin also protects the human body from physical and mechanical aggressions through its flexibility and toughness.

Besides the physical protection, the skin can acts as a chemical barrier by presenting several substances that prevent the proliferation of harmful microorganisms. For instance, the sebaceous lipids produced by the sebaceous glands antibacterial properties. These substances prevent the invasion of the skin by pathogenic microorganisms reducing the risk of infections in the skin. The skin also has an important function in the immunological system. There are cells responsible for the recognition of antigens located in the skin. Thus, the cells of the skin are strongly related with the immunological response.

Human skin also presents mechanisms to minimize the effects of the UV radiations from the sun. UV radiation is responsible by sunburns and has an important role in premature skin aging and in skin cancer development. The skin presents two barriers to protect us from the UV rays. These two barriers absorb the UV radiation reducing the absorption by DNA and other cellular constituents. One of these barriers is formed by melanin and the other barrier is formed by proteins. Additionally, the lipids in the skin also may contribute to protection from UV rays. Furthermore, when skin is exposed to sunlight, it not

only absorbs radiation but also produces vitamin D which is a very important chemical substance for the human body.

Another important function of the skin is to maintain the human body temperature. The skin presents several cells sensitive to variations in temperature. The information received by these cells leads to the stimulation or inhibition of sweating or shivering. Also, when the temperature decreases, the blood flow in the skin increases and this avoids the heat loss to the environment.

In addition to being sensitive to temperature variations, the skin is also sensitive to several different sensorial stimuli. The skin has a very dense network of nerve fibers and nerve endings. Through this network, the sensory nervous system may perceive the sensations of touch, vibration, pressure, pain, itch, and changes in temperature as mentioned previously. Because of this sensibility to different types of stimuli, the skin acts as a sensory organ and has an important role in the human communication. The appearance, smell, and feel of the skin are also an important factor in the social and sexual human communication.

It should be noted that these functions of the skin may vary from one individual to another. For instance, the skin of old people loses flexibility and toughness. People with dark skin have higher protection to UV radiation than people with fair skin. In other words, the skin functions depend on factors such as age, race, and other individual characteristics.

3.2 Skin Structure

The skin consists of two layers: the most superficial layer called epidermis, and an underneath layer called dermis. More deeply, right after the dermis there is a layer of subcutaneous fat, which is separated from the rest of the body by a muscle layer. Figure 3.1 illustrates the human skin organization. We have to note that the subcutaneous fat layer is not considered a skin layer. Only epidermis and dermis form the skin. The subcutis is a flexible layer and its fat cells act like a shock absorber for blood vessels and nerve endings.
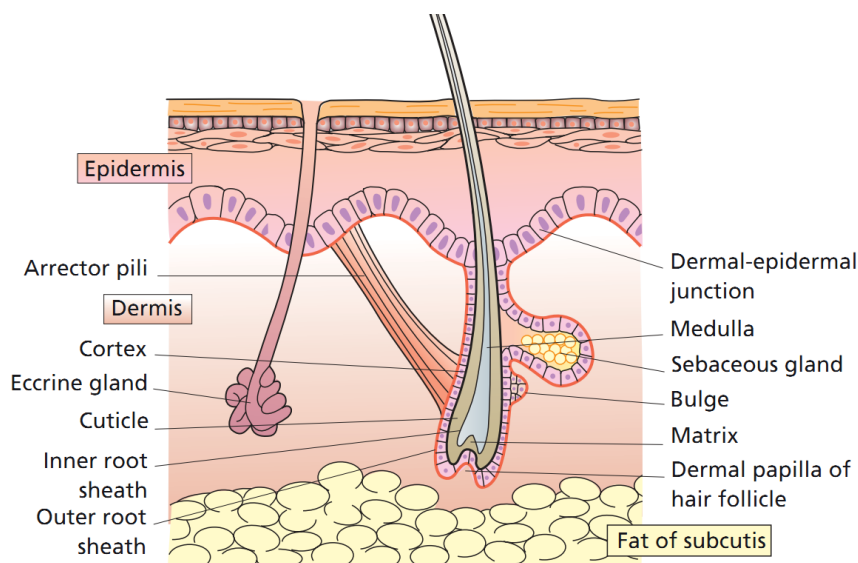
Figure 3.1: Human skin organization (BURNS et al., 2010).

3.2.1 Dermis

The dermis is delimited on top by the basement membrane (see Figure 3.2) which separates epidermis and dermis. On the bottom, the dermis is delimited by the subcutis. The dermis constitutes the major part of human skin and is formed mainly by an extracellular matrix of connective tissues and a complex meshwork of various macromolecules. In this sense, the dermis has almost no cells. There are four main categories of dermis components: collagen fibers which are responsible by the skin toughness that gives to the skin the ability to protect against external traumas; the structures which provides to skin elasticity; proteins which organize and help the cell-matrix interactions; and macromolecules responsible by the hydration of the skin.

3.2.2 Epidermis
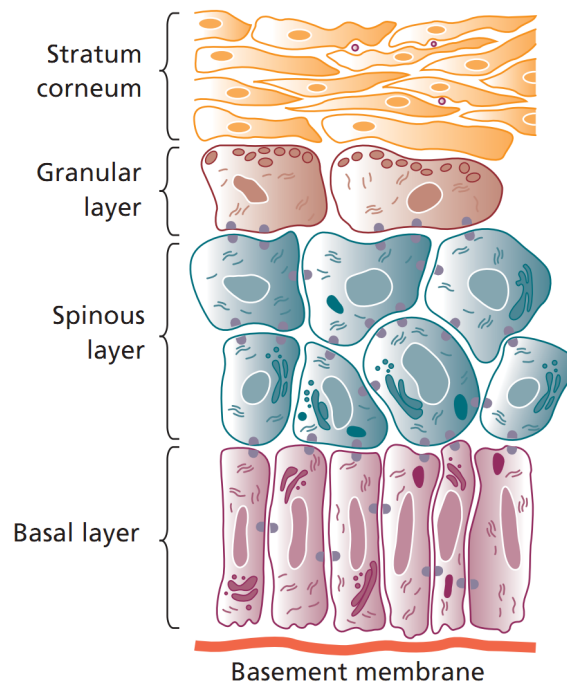
Figure 3.2: Epidermis layers (BURNS et al., 2010).

The epidermis is formed mainly by keratinocytes. Around 95% of the epidermis are keratinocytes. Keratinocytes move upward from the epidermal basement membrane to the skin surface. In this process, which takes around four weeks, the keratinocytes change their structures and functions forming several different layers. Thus, the epidermis can be subdivided accordingly to these layers which are four: basal layer, spinous layer, granular layer, and stratum corneum. Figure 3.2 shows the layers of epidermis.

Right below the epidermis lies the basement membrane. The basement membrane is a thin sheet of fibers and controls the transportation of cells and substances between the dermis and epidermis. Thus, since the epidermis is avascular, the nutrients required by the epidermis move from dermis to epidermis through this membrane.

3.2.2.1   Basal Layer

The basal layer is the deepest layer of epidermis and it constitutes the boundary to the dermis. This layer is continuous and usually with just one cell thick. However, in some regions it may have two or three cells thick. Keratinocytes are produced in this layer. Melanocytes are also located in this layer.

3.2.2.2   Spinous Layer

The spinous layer is formed by between 10 to 20 layers of keratinocytes cells above the basal layer. These keratinocytes are produced in the basal layer and after being produced they change their shape into a polyhedral form.

3.2.2.3   Granular Layer

The granular layer is where the keratinization of keratinocytes occurs. In keratinization the cells are filled with keratin fibers. This process makes the keratinocytes shape turn into a flatter shape. Also in this process, the lipid components of the cells are discharged into intercellular space. These lipids have an important role in the barrier function of the skin making it waterproof. These lipids are also important to the cohesion of the cells in the above epidermis layer.

3.2.2.4   Stratum Corneum

Stratum corneum is the outermost epidermis layer. In this layer, the cells have lost their organelles and are filled with keratin. These changes in the content inside the cells make their shape become even flatter. This epidermis layer is responsible by the water loss avoidance. So, this epidermis layer keeps the skin hydrated. Actually, this layer contains between 10% and 15% of total water mass in the epidermis.

3.3   Main Skin Cells

The skin presents several different types of cells. However, for the purpose of our work, we only need to understand the role of melanocytes and keratinocytes in the human skin. Thus, in this section, we detail these two cells.

3.3.1   Keratinocytes

Keratinocytes are the more abundant cells in the epidermis. They are responsible by the keratin production. Keratin is a protein that contributes to the skin surface rigidity. Keratinocytes are involved in several protection functions of the skin. Keratinocytes contributes to protection of the body against friction, viruses and other several harmful factors. Also, keratinocytes are primarily responsible for skin impermeability. Keratinocytes also has an important role in the skin regeneration. When the skin presents a wound, the keratinocytes migrates to fill the space caused by this would.

Keratinocytes can be classified in four different types of cells depending on where in the epidermis they are located. In addition, each type of keratinocytes presents different functions and structures. The four types of keratinocytes are: basal cells, spinous or prickle cells, granular cells, and horny cells. These cells are located respectively in basal layer, spinous layer, granular layer, and stratum corneum.

The keratinocytes also receive melanin from the nearby melanocytes packed in organelles called melanosomes (see Figure 3.3). The function of melanin in keratinocytes

is to absorb the UV radiation and avoid that this radiation penetrates deeper in the skin. As the keratinocytes move up in epidermis and change from a type to another, the melanosomes suffer a degradation process. However, the production of melanosomes by melanocytes is a constant process as the process regarding the keratinocytes renewal. Thus, new keratinocytes receive new melanosomes from the nearby melanocytes in the basal layer keeping the skin protection against the UV rays through the melanin.

3.3.2 Melanocytes
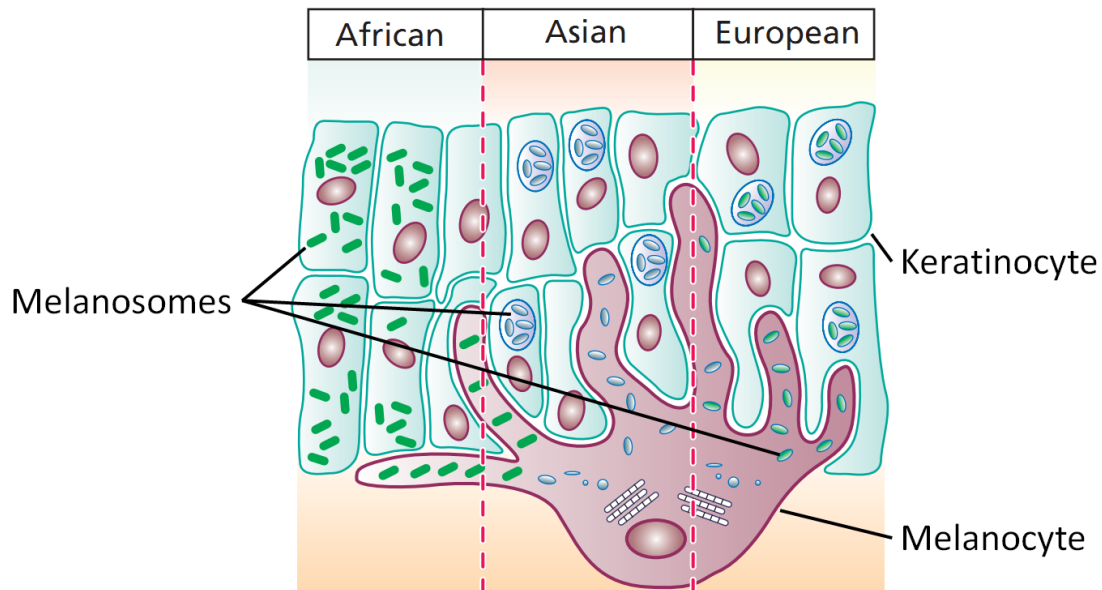
Figure 3.3: Melanocyte (BURNS et al., 2010).

Melanocytes are cells responsible for production of pigments which determine the color of skin, hair, and iris of eye. The melanocytes produce two types of melanin: eumelanin (brown/black) and phaeomelanin (yellow/red). Variations in type and distribution of melanin contribute to the several different human shades of hair, skin, and eye colors. In the skin, melanocytes are located in basal layer of epidermis. The melanin produced in this layer provides the skin protection from UV rays.

The produced melanin is packed into melanosomes. After that, the melanosomes are transferred to surrounding keratinocytes in the epidermis and to hair follicles. The effective melanosomes transfer depends on the melanocytes dendrites. Figure 3.3 shows the structure of a melanocyte and its dendrites connecting the nearby keratinocytes. This production of melanin and its packing into melanosomes are stimulated by the UV radiation. The transfer of melanosomes to keratinocytes is also stimulated by the UV rays. Currently, the process by which melanosomes move from melanocytes to keratinocytes is not fully understood (BURNS et al., 2010).

The number of melanocytes varies slightly between the different races and sexes. People of dark skin have a greater capacity in synthesis and transfer of melanosomes than people with fair skin. As we can see in Figure 3.3, the differences involving the pigmentation distribution in different races are related with melanosomes organization and not with amount of melanin. Thus, in Figure 3.3 we can observe that melanosomes in Africans are more widely spread than in Europeans and Asians. Although the distribution of melanosomes vary slightly in different races, different skin regions in human body

present significant variation of melanocytes distribution. Usually, skin in regions more exposed to sun light, such as face and arms, present a higher concentration of melanocytes. Figure 3.4 shows the variation of melanocytes number in different skin regions of human body.
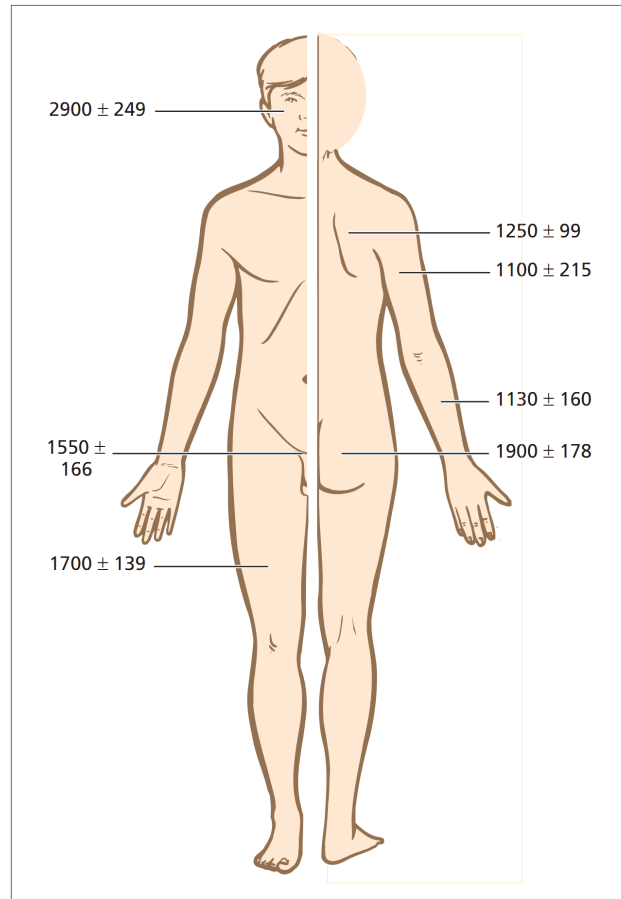
Figure 3.4: Regional variation of melanocytes distribution in epidermis (BURNS et al., 2010). Values represents the mean number of melanocytes by mm^2± standard error of the mean.

3.4 Pigmentation Disorders

In our work, we concentrate only on pigmentation disorders related with the melanocytes proliferation and the production of melanin by these melanocytes. Thus, we do not consider pigmentation disorders caused by: external factors such as chemical substances, drugs, tattoos, skin wounds, scars, and skin burns; abnormal functions of human body which are external to epidermis but that influence in the life cycle of the melanocytes or keratinocytes such as the hypotheses for the causes of vitiligo; and the different sizes and organizations of melanocytes and melanosomes in the skin as we found in freckles (BARNHILL; PIEPKORN; BUSAM, 2004). As consequence, in our work we simulate the following pigmentation disorders: lentigines, melanoma and idiopathic guttate hypomelanosis (IGH). In this section, we detail these three human pigmentation disorders.

3.4.1 Lentigines

Figure 3.5: Lentigines (BURNS et al., 2010).

Melanocytes maintain a constant contact with the keratinocytes which they transfer melanosomes. Some disorders may have their origin in the proliferation of benign melanocytes. When this proliferation is formed by melanocytes able to produce melanin, a hyperpigmented lesion called lentigo arises in the skin.

Lentigines are small round or oval areas of dark pigmentation in the skin. Also, several individual lentigines can agglutinate in a larger lentigo with a more irregular shape. Lentigo is a lesion that may persist for a long time and do not disappear in winter as sometimes is observed in a freckle. When a lentigo is observed under a microscope, the number of melanocytes in the basal layer of epidermis is significantly greater than the number of melanocytes expected for the skin region evaluated.

Lentigines are more frequently observed in people with fair skin. The lentigines are usually the response of melanocytes to the sun exposure. However, sometimes the lentigines occurrence is associated with causes unrelated to the sun light exposure such as in leopard syndrome. Figure 3.5 shows several lentigines in the leg of a patient.

3.4.2 Melanomas

Since the melanocytes are in the epidermis, the most superficial skin layer, sometimes the UV radiation damages their DNA structure and they suffer a malignant transformation. This transformation sometimes makes the melanocytes proliferate faster than normal and leads to the development of malignant skin lesions called melanoma. As the lentigines, melanomas are also pigmentation disorders categorized as hypermelanosis and are also more frequently observed in people with fair skin.

In most cases the melanoma proliferation remains limited to the epidermis for some time before the transformed melanocytes gain the ability for proliferate and survive in the dermis. After reaching dermis, melanoma may fall into a blood vessel and spread through the other organs of human body. This process is called metastasis.

Figure 3.6: Melanoma (BURNS et al., 2010).

Melanomas may be diagnosed by the American ABCD diagnostic system. This diagnostic system is very popular and was developed aiming to help the recognition of melanomas by non-experts and the general public. The ABCD letters represents the main characteristics of a melanoma which are: A = asymmetry, B = irregular border, C = irregular color, and D = diameter greater than 1 cm. Figure 3.6 shows an example of melanoma.

3.4.3 Idiopathic Guttate Hypomelanosis

According to (NEW ZEALAND DERMATOLOGICAL SOCIETY INCORPORATED, 2011), IGH affects mostly the fair-skinned people. It appears more frequently in skin regions more susceptible to sun light exposure and is more common in old people than in young people and in women than in men.

As the name suggests, IGH is classified as a hypomelanosis type of pigmentation disorder. IGH is characterized by white spots having size around 2 to 5 mm. The causes of IGH are speculative. However, it has been suggested that this disorder results from a melanocytes mutation. In the IGH lesions there is no pigment in the keratinocytes. Also, there is a reduction in the number of melanocytes in the lesions and most of these melanocytes have no mature melanosomes. The small white spots in Figure 3.7 illustrate the effects of IGH.

Figure 3.7: Idiopathic guttate hypomelanosis (NEW ZEALAND DERMATOLOGICAL SOCIETY INCORPORATED, 2011).

3.5 Summary

In this chapter we listed the main functions of the human skin. We showed that the skin has several important roles to the maintenance of human body integrity. Also, the skin has an important participation in the human communication and interactions as it represents one of our sensory organs.

We also presented the structure of the skin. We detailed the two skin layers, dermis and epidermis, and we explained the functions, organization and compounding parts of the dermis and epidermis. Also, we described the two most important cells to the understanding of the pigmentation disorders addressed in our work, which are the keratinocytes and the melanocytes.

In addition, we explained the characteristics and mechanisms behind the pigmentation disorders simulated in our work. Two of these disorders are classified as hypermelanosis: lentigines and melanoma. The remaining pigmentation disorder is classified as hypomelanosis and is called idiopathic guttate hypomelanosis.

Thus, in this chapter we presented the biological knowledge regarding the human skin and some human pigmentation disorders. The information presented in this chapter is important to the understanding of the developed simulation model presented in the next chapter.

4 SIMULATION MODEL

In this chapter we present the main contribution of our work which is a biologically inspired mathematical model to simulate the most frequent types of human skin pigmentation disorders. As mentioned in Chapter 3, we are focusing in the pigmentation disorders related to melanocytes proliferation. Sometimes, this proliferation is a normal organism response to specific stimuli such as the excessive UV radiation exposure. In this case, this proliferation is called hyperplasia and this is the process behind the lentigines (NORDLUND et al., 2006). However, the melanocytes proliferation process also occurs in an abnormal manner. In this case, this process is called neoplasia (COTRAN et al., 1999) and this is the process behind benign skin tumors and skin cancers such as melanoma. Additionally, also as mentioned in Chapter 3, we know that the epidermis is an avascular skin layer. Accordingly, our model has to deal with proliferation of cells in an avascular environment.

Different approaches can be used to model scenarios involving cells proliferation in avascular environments. However, differential equations systems have been traditionally and successfully used to model these scenarios. These mathematical systems were used to model scenarios such as bacterial growth (BARANYI; ROBERTS, 1994; BARANYI; ROBERTS; MCCLURE, 1993; SPICER, 1955), fungi proliferation (KIDER; RAJA; BADLER, 2011), and avascular cancers (KONUKOGLU et al., 2010; KHAIN; SANDER, 2006; FERREIRA JR.; MARTINS; VILELA, 2002; GATENBY; GAWLINSKI, 1996). Therefore, we also use a differential equations system to model human skin pigmentation disorders. The goal of this system of equations is to reproduce the effects of pigmentation disorders caused by the proliferation of melanocytes. More specifically, our system has to simulate the interactions of different populations of melanocytes in the epidermis. Each population presents different mutations or alterations. For instance, in our model we assume that the IGH characteristics spots are produced by a population of melanocytes which presents a mutation that makes them unable of produce melanosomes and melanin. In short, the simulation model proposed in this work has to generate skin lesions resulting from IGH, lentigines, and melanomas. The differential equations used in our simulation model are explained in Section 4.1 The assumptions of our model are summarized in Section 4.2. The method used to solve these equations is explained in Section 4.3. Further, the properties of our simulation model are presented in Section 4.4. We describe and show the results of a validation process applied to our simulation model in Section 4.5. In Section 4.6 we discussed other simple approaches that could be used to produce results that are similar to our results.

4.1 The Differential Equations System

The main output of our model is the melanosomes distribution in an epidermis region. More specifically, we consider the epidermis is a two-dimensional surface and we use our system of equations to calculate the amount of melanosomes in each point of this surface at a given instant of time. The melanosomes concentration is represented by the function M. Based on biological information regarding the melanosomes, we consider that the number of melanosomes is related to the number of melanocytes producing melanosomes and related to the excitation level of these melanocytes. In our model, there are two types of melanocytes which produce melanosomes: the healthy melanocytes proliferating at a normal speed; and the melanocytes which participate in the processes of hyperplasia or neoplasia and proliferate faster than normal melanocytes. The number of normal melanocytes is represented by the function N and the number of melanocytes proliferating faster is represented by function F. We also consider that the melanocytes excitation level, represented by function E, affects uniformly all the melanocytes in a given point over the epidermis at a specific time instant. We use this excitation level to model external stimuli that alter the production of melanosomes such as solar radiation. Accordingly, we calculate the variation of melanosomes over the time by the following equation:

$$\frac{\partial M}{\partial t} = E(N + F) - P_{md}M + D_m\nabla^2 M$$

where $D_m\nabla^2 M$ is used to model the melanosomes spreading to the surrounding keratinocytes via the melanocytes dendrites. In addition, $P_{md}M$ represents the portion of melanosomes that are degraded because of the keratinocytes upward movement inside the epidermis.

As we age, the number of melanocytes tends to decrease slightly (BURNS et al., 2010). But, for simplicity, in our model we assume that the number of normal melanocytes remains constant in a healthy skin region. Alternatively, the amount of normal melanocytes in a non-healthy skin region only decreases. This happens because normal melanocytes may mutate and become melanocytes that: reproduce faster than normal, or do not produce melanosomes, or both. In other words, any alteration undergone by a melanocyte causing it to behave differently from normal decreases the normal melanocytes population. The amount of normal melanocytes can also decrease by effect of the increasing population of the mutated melanocytes which can suppress the normal melanocytes population since these populations of melanocytes have to compete for nutrients and space. Therefore, the following equation represents the variation of normal melanocytes in the simulation model:

$$\frac{\partial N}{\partial t} = -P_{nb}N - P_{nf}N - P_{nw}N - S_{bn}B - S_{fn}F - S_{wn}W + D_n\nabla^2 N$$

where $P_{nb}N$, $P_{nf}N$, and $P_{nw}N$ represent the portion of normal melanocytes that suffers the different mutations considered in our model. Also, $S_{bn}B$, $S_{fn}F$, and $S_{wn}W$ represent the suppression effect by the others melanocytes populations. Finally, the term $D_n\nabla^2 N$ models the diffusion of normal melanocytes in basal skin layer.

As mentioned above, in our model we consider that the melanocytes can suffer two different alterations or mutations. One of these mutations makes the melanocytes reproduce faster than normal. This is the process behind the lentigines and melanomas. In this situation, the melanocytes population grow in a region of the epidermis and this makes

the amount of melanosomes in this region to increase. Thus, the high concentration of melanosomes in a skin region leads to the appearing of dark spots which could be lentigines or melanomas. The other mutation makes the melanocytes stop the melanosomes production. The lack of melanosomes in a skin region leads to the formation of the IGH characteristic white spots. As mentioned in Chapter 3, the causes of IGH are speculative but a recurring hypothesis is the presence of a mutation in the melanocytes that makes them unable to produce mature melanosomes. Thus, we assume the presence of this mutation in our model. Also, in our model we consider that a melanocyte can have these both mutations simultaneously. In short, in our model we have four different populations of melanocytes: normal melanocytes, melanocytes that reproduce faster, melanocytes unable of produce melanosomes, and melanocytes that reproduce faster and do not produce melanosomes.

Regarding the population of melanocytes that are incapable of producing melanosomes, we assume that this population reproduces at the same rate that normal melanocytes population. Also, this population can decrease because of the suppression effect from the other melanocytes populations, This population also decrease when a melanocyte acquires the other mutation and become part of the population of melanocytes with both mutations. However, differently from normal melanocytes population, we assume that this population may increase when a normal melanocyte mutates and becomes a melanocyte that does not produce melanosomes. The function W represents the population of melanocytes without melanosomes production and the variation of this population is given by:

$$\frac{\partial W}{\partial t} = P_{nw}N - P_{wb}W - S_{bw}B - S_{fw}F - S_{nw}N + D_w\nabla^2 W$$

where: $P_{nw}N$ represents the portion of normal melanocytes that became unable to produce melanosomes; $P_{wb}W$ represents the melanocytes unable to produce melanosomes that became melanocytes with both mutations. $S_{bw}B$, $S_{fw}F$, and $S_{nw}N$ represent the suppression by the other melanocytes population; and $D_w\nabla^2 W$ represents the slight movement that the melanocytes from this population may perform in epidermis. By disregarding external influences, we assume that this population remains constant over time in the same way that the normal melanocytes population. Thus, there is an equilibrium related to the number of melanocytes that are produced and the number of melanocytes that die in this population. Because of this equilibrium, the above equation does not need a growth term as well as the equation related to the variation of normal melanocytes population.

Differently from the above described melanocytes populations, which remains constant over time if not influenced by external factors, the population of melanocytes that reproduces faster than normal may increase over time until they reach a maximum limit. We have two populations with this feature: the population of melanocytes that only reproduce faster than normal, and the population of melanocytes that not only reproduce faster but also are incapable to produce melanosomes.

The variation in the population of melanocytes that only reproduces faster is described by the equation

$$\frac{\partial F}{\partial t} = P_{nf}N - P_{fb}F + G_f F - \frac{G_f F^2}{L_f} - S_{bf}B - S_{nf}N - S_{wf}W + D_f\nabla^2 F$$

where, as mentioned previously, the function F represents the size of the population of

melanocytes that reproduce faster. In addition, the population of melanocytes that reproduce faster and cannot produce melanosomes is described by the equation

$$\frac{\partial B}{\partial t} = P_{fb}F + P_{nb}N + P_{wb}W + G_bB - \frac{G_bB^2}{L_b} - S_{fb}F - S_{nb}N - S_{wb}W + D_b\nabla^2B$$

where the function B represents the population with both mutations. G_fF and G_bB are the population growth terms and they represent respectively the growth of F and B. This terms model the melanocytes multiplication through mitosis. $-\frac{G_fF^2}{L_h}$ establishes the limit to the growth of F. In the same way, $-\frac{G_bB^2}{L_b}$ defines the maximum limit to the population represented by B. The portion of N that mutates into F is represented by the term $P_{nf}N$. Analogously, $P_{fb}F$ represents the portion F that mutates into B and so on. Also, the term $S_{bf}B$ represents the suppression effect of B into F, $S_{nf}N$ represents the suppression effect of N into F, and so forth. Finally, $D_f\nabla^2F$ represent the spreading of F and $D_b\nabla^2B$ the spreading of B.

4.2 Model Assumptions

In short, based on current biological knowledge, our model was developed considering the following assumptions:

- The number of melanosomes is proportional to the number of melanocytes and the excitation level of these melancytes.

- The excitation level is determined by an external stimuli (such as the sun light exposure) which uniformly affects all the melanocytes in a specific skin region.

- There is a mutation that causes the melanocytes stop the melanosomes production.

- The reproduction and mortality rate of healthy melanocytes and melanocytes that are incapable of melanosomes production are the same so these populations of melanocytes remain constant over time if not disturbed by external factors.

- The reproduction rate of the remaining melanocytes populations of our model is greater than their mortality rate.

4.3 Solving The Differential Equations

Our proposed differential equations system can be rewritten as

$$\begin{pmatrix} \frac{\partial M}{\partial t} \\ \frac{\partial N}{\partial t} \\ \frac{\partial W}{\partial t} \\ \frac{\partial F}{\partial t} \\ \frac{\partial B}{\partial t} \end{pmatrix} = \begin{pmatrix} E(N+F) - P_{md}M \\ -P_{nb}N - P_{nf}N - P_{nw}N - S_{bn}B - S_{fn}F - S_{wn}W \\ P_{nw}N - P_{wb}W - S_{bw}B - S_{fw}F - S_{nw}N \\ P_{nf}N - P_{fb}F + G_fF - \frac{G_fF^2}{L_f} - S_{bf}B - S_{nf}N - S_{wf}W \\ P_{fb}F + P_{nb}N + P_{wb}W + G_bB - \frac{G_bB^2}{L_b} - S_{fb}F - S_{nb}N - S_{wb}W \end{pmatrix} +$$

$$
\begin{pmatrix}
D_m & 0 & 0 & 0 & 0 \\
0 & D_n & 0 & 0 & 0 \\
0 & 0 & D_w & 0 & 0 \\
0 & 0 & 0 & D_f & 0 \\
0 & 0 & 0 & 0 & D_b
\end{pmatrix}
\begin{pmatrix}
\nabla^2 M \\
\nabla^2 N \\
\nabla^2 W \\
\nabla^2 F \\
\nabla^2 B
\end{pmatrix}
$$

and considering

$$
\mathbf{q} =
\begin{pmatrix}
M \\
N \\
W \\
F \\
B
\end{pmatrix},
$$

$$
\mathbf{r} =
\begin{pmatrix}
E(N + F) - P_{md}M \\
-P_{nb}N - P_{nf}N - P_{nw}N - S_{bn}B - S_{fn}F - S_{wn}W \\
P_{nw}N - P_{wb}W - S_{bw}B - S_{fw}F - S_{nw}N \\
P_{nf}N - P_{fb}F + G_f F - \frac{G_f F^2}{L_f} - S_{bf}B - S_{nf}N - S_{wf}W \\
P_{fb}F + P_{nb}N + P_{wb}W + G_b B - \frac{G_b B^2}{L_b} - S_{fb}F - S_{nb}N - S_{wb}W
\end{pmatrix},
$$

and

$$
\mathbf{D} =
\begin{pmatrix}
D_m & 0 & 0 & 0 & 0 \\
0 & D_n & 0 & 0 & 0 \\
0 & 0 & D_w & 0 & 0 \\
0 & 0 & 0 & D_f & 0 \\
0 & 0 & 0 & 0 & D_b
\end{pmatrix}
$$

we have

$$
\frac{\partial \mathbf{q}}{\partial t} = \mathbf{r} + \mathbf{D}\nabla^2 \mathbf{q}
$$

which is the general form of a reaction-diffusion system. In reaction-diffusion systems, $\mathbf{q}$ is a vector of functions that determine the concentration of a given element, in our case the elements of the system are the different melanocytes populations and the melanosomes; $\mathbf{r}$ represents the local interactions or "reactions" involving the elements of the system; and $\mathbf{D}$ represents the spatial spread or "diffusion" of these elements.

Analitic solutions of reaction-diffusion systems are difficult or impossible to obtain except when the interactions involving the elements of the system are very simple (TURK, 1992). Because of this, reaction-diffusion systems are usually solved through a numerical method. For simplicity, the explicit or forward Euler method is very popular for reaction-diffusion systems. This method has been traditionally and successfully used in several works such as (JIMÉNEZ; STEINBOCK, 2012), (SEN; GHOSH; RAY, 2010), (WANG

et al., 2010), and (WITKIN; KASS, 1991). For this reason, we also use the forward Euler method in our work. In future work, we plan to use faster multigrid techniques.

Our numerical simulations are performed in a two-dimensional space and moving forward in time. The space is discretized in squared grid elements of equal size and time in steps of equal duration. We use periodic boundary conditions.

Based on the biological data provided by (BURNS et al., 2010) we know that 1000 melanocytes per mm^2 is a concentration that is feasible and consistent with real human skin data. We decide to have a resolution of 100 grid elements per mm^2 because this value provides a good balance between the quality of the output and its processing time. Thus, to provide this resolution while keeping 1000 melanocytes per mm^2, in our system, each grid element starts with 10 normal melanocytes. Regarding the concentration of melanosomes in the skin, only recently (NIELSEN et al., 2008) proved that it is possible to calculate the melanosome concentration in the epidermis from its reflectance spectra by using an accurate discrete ordinate radiation transfer model with a classical inversion scheme based on Bayesian optimal estimation theory for retrieval of parameters. However, this work does not provide data that could be used to estimate the amount of melanosomes in a specific skin area. Because of this lack of data, we empirically defined the starting melanosomes concentration as 60 melanosomes per grid element based on the proportion of keratinocytes per melanocyte in the epidermis. Also because of this lack of biological data, the reaming parameters of our model were empirically defined in order to simulate pigmented lesions that have the same characteristics of real pigmented lesions. In short, in our system, each grid element starts with 10 normal melanocytes and 60 melanosomes which are produced by the 10 normal melanocytes. Thus, the initial value of N is 10 and M is 60 for each grid element in the entire two-dimensional space of the simulation. The other melanocytes populations start with 0 melanocytes.

For all results shown in this work, we define E and P_{md} as constant functions where $E = 0.6$ and $P_{md} = 0.1$ and this makes the amount of melanosomes remains constant in epidermis regions that only present normal melanocytes. All the suppression terms are also constant functions. $S_{bn} = 0.002$, $S_{bf} = 0.2$, $S_{fn} = 0.02$, and the remaining suppression terms were set as 0.

G_b and G_f are functions of the two spatial dimensions of the simulation then, as a consequence, $G_b = f_{G_b}(x, y)$ and $G_f = f_{G_f}(x, y)$ where x and y represent the two spatial dimensions of the simulation. G_b and G_f return random uniformly distributed values between 0 and 0.2. This variation in the growth terms of the equations models the slight differences in the distribution of nutrients and other factors that interferes in the melanocytes life cycle. L_b and L_f, which establish the limits to the growth of B and F, were set as 300.

The terms P_{fb}, P_{nb}, P_{nf}, P_{nw} and P_{wb} which model when a melanocyte suffers a mutation are functions of the two space dimensions and the time. In other words, these functions determine where and when the melanocytes mutate. These functions are different depending on the desired results. However, they usually return random values accordingly with some probability distribution.

Usually, in the reaction-diffusion systems, the diffusion is guided by a unique diffusion coefficient for each element in the system. However, the diffusion coefficient can be replaced by diffusion functions. Sometimes, this is done to induce movement in a specific direction or set of directions. The usage of diffusion functions instead of diffusion coefficients was found in (KARDASHOV et al., 2006) and, as this work, we also use diffusion functions. These functions take the form $f(x, y)$ and are used to determine regions

where de movement of the melanocytes is easier or not. Basically, these functions define different diffusions coefficients for each grid element in the simulation. Thus, they can model the possible obstacles encountered by the melanocytes which reproduce faster than normal and guide the process that defines the shape of a pigmented lesion. The definition of these diffusion functions are influenced by the desired type of lesion that we want to produce. Likewise the functions that determine the melanocytes mutations, the diffusion functions return random values accordingly to probability distributions.

In Table 4.1 we summarize the roles of every term used in the equations of the reaction-diffusion system. Also, in this table, we show all the values assigned by default to these terms before we start to run the simulation. Not all values terms are usually considered in a default simulation scenario. However, they can be manually set in order to reproduce some desired effect.

term	role in the system	default/initial value
M	melanosomes concentration	60
N	normal melanocytes	10
W	melanocytes without melanosomes	0
F	melanocytes that reproduce faster	0
B	melanocytes with both mutations	0
E	melanocytes excitation	0.6
G_f	growth of F	random values uniformly distributed between 0 and 0.2
G_b	growth of B	random values uniformly distributed between 0 and 0.2
L_f	limit of F population	300
L_b	limit of B population	300
P_{md}	portion of melanosomes that are degraded	0.1
P_{nb}	portion of N that mutates into B	randomly defined so that 1 in 50000 cells receives a value uniformly distributed between 0 and 0.001
P_{nf}	portion of N that mutates into F	randomly defined so that 1 in 250000 cells receives a value uniformly distributed between 0 and 0.001
P_{nw}	portion of N that mutates into W	0
P_{fb}	portion of F that mutates into B	0
P_{wb}	portion of W that mutates into B	0.6
S_{bn}	suppresion of B into N	0.002
S_{fn}	suppresion of F into N	0.02
S_{wn}	suppresion of W into N	0
S_{bw}	suppresion of B into W	0
S_{fw}	suppresion of F into W	0
S_{nw}	suppresion of N into W	0
S_{bf}	suppresion of B into F	0.2

term	role in the system	default/initial value
S_{nf}	suppresion of N into F	0
S_{wf}	suppresion of W into F	0
S_{fb}	suppresion of F into B	0
S_{nb}	suppresion of N into B	0
S_{wb}	suppresion of W into B	0
D_m	diffusion of melanosomes	0.2
D_n	diffusion of normal melanocytes	0.05
D_w	diffusion of melanocytes without melanosomes	0.05
D_f	diffusion of melanocytes that reproduce faster	defined in a way that around half of the cells present random diffusion coefficients uniformly distributed between 0 and 0.000002 and the other half between 0 and 0.03.
D_b	diffusion of melanocytes with both mutations	defined in a way that around half of the cells present random diffusion coefficients uniformly distributed between 0 and 0.000002 and the other half between 0 and 0.03.

Table 4.1: Model summary.

4.4 Model Properties

Our model is able to simulate skin lesions in different stages of development. This feature was not present in any of the works reviewed in Chapter 2. To obtain a different stage of development of a lesion we just have to process more time steps of the reaction-diffusion system. We can see the evolution of hyperpigmented and hypopigmented lesions. Sometimes, two small lesions growth and agglutinate forming a bigger lesion. As described in Chapter 3, this is a phenomenon that also occurs with real lesions. In Figure 4.1 we have the temporal evolution of a hyperpigmented lesion.
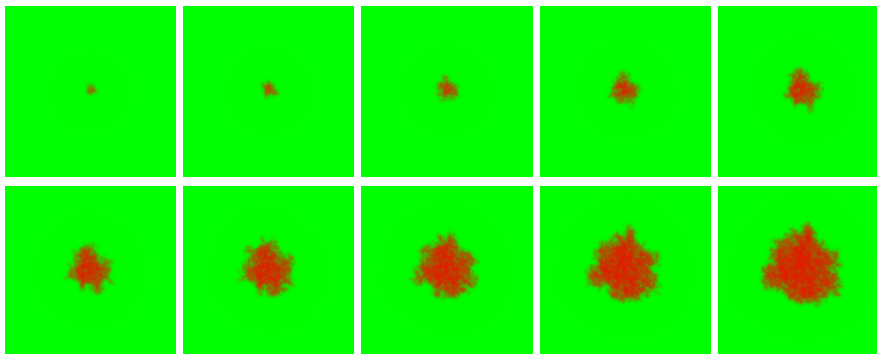

Figure 4.1: Temporal evolution of a hyperpigmented lesion.

In real pigmented lesions, particularly in melanomas, we found different shades of colors. These differences are consequence of nonuniform melanosomes distributions inside the lesions. We reproduce this variation in the melanosomes distribution by varying the values of the growth factors of our reaction-diffusion system. Thus, the greater the variation in the growth factors, the greater is the variation in the melanosomes concentration. As described in previous section, G_b and G_f return random uniformly distributed values between 0 and 0.2. These values are used in all simulations presented in this work. However, in Figure 4.2, we alter G_f to illustrate the effect of changing the growth factors in the simulation.
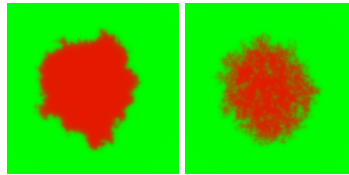

Figure 4.2: Varying the melanosomes distribution. Left image is the result of a simulation with $G_f = 0.2$ and in the right image G_f returns random values uniformly distributed between 0 and 0.3.

Pigmented lesions are presented in different shapes. Usually, the benign lesions present a more regular border and the malignant lesions present a more irregular border. We control the shape of the lesions by the diffusion term of our reaction-diffusion system. As described in previous section, we use diffusion functions instead of diffusion values in our reaction-diffusion system. These functions define different diffusion coefficient for each cell in the simulation. When there is a slight variation in the diffusion values from cell to cell, the border of the lesions will be more regular. However, when this variation is higher, we have lesions with a more irregular border. In figure 4.3 we present the result of this variation in the diffusion coefficients.
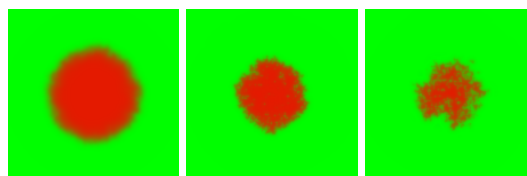
Figure 4.3: Results of using different diffusion functions. From regular to irregular borders.

4.5 Model Validation

Irregular borders and asymmetry are features of pigmented lesions that are frequently used for diagnosis purposes. These features are evaluated not only manually by dermatologists but also by several automated tools. These tools aim to categorize the pigmented lesions based on metrics extracted from features of the lesions. The production of such tools is a much explored topic in dermatology. (SCHMID-SAUGEONA; GUILLODB; THIRANA, 2003) and (ALCÓN et al., 2009) present automated methods to support the

diagnosis of pigmented lesions that include the evaluation of asymmetry and borders irregularities. Also, (ZHOU et al., 2010a) and (LEE, 2001) use only the evaluation of borders irregularities and (STOECKER; LI; MOSS, 1992) uses only the evaluation of asymmetry in pigmented lesions. Because of recurrent usage of border irregularities and asymmetry in inspection of pigmented lesions, in order to evaluate the quality of our results, we compare our results with real pigmented lesions images by assessing the border irregularities and the asymmetry. To the best of our knowledge, our work is the first that defines a method to evaluate the quality of simulated pigmented lesions.

Regarding the asymmetry, we use the same approach used in (STOECKER; LI; MOSS, 1992). In this work, they compute the two orthogonal symmetry axes of the lesion using the principal component decomposition of a binary mask of the lesion. Further, they compute the asymmetry index for both axes by using

$$\frac{\Delta A}{A},$$

where ΔA represents the nonoverlapping area between the original mask and its reflection relative to the asymmetry axis, and A is the area from the original mask. In (STOECKER; LI; MOSS, 1992), this computation is done for both symmetry axes but only the minimum value is kept. In our work, we use both values for comparison. Figure 4.4 shows the computation steps of the asymmetry index.
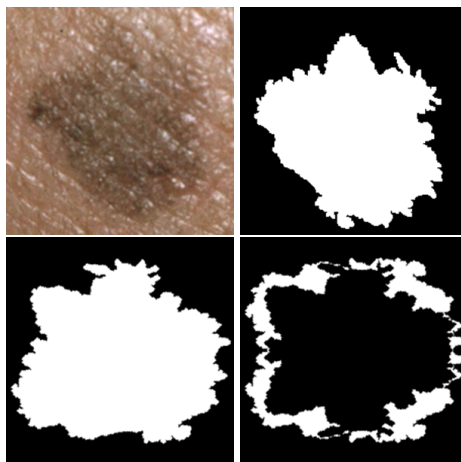

Figure 4.4: Calculation steps of the asymmetry index. We start with a real lesion image or a simulation result (left top image). Next, we compute a binary mask which separates the lesion from the background (right top image) so we find the two orthogonal asymmetry axis of this binary mask by using principal component decomposition. In left bottom image, the binary mask was rotated until the asymmetry axes align with the vertical and horizontal axes of the image. After that, the binary mask is reflected relative to both asymmetry axes. Finally, we calculate the nonoverlapping area between the binary mask and its reflections and we divide these calculated areas by the area of the original binary mask. Right bottom image shows the nonoverlapping relative to horizontal axis.

Regarding the border irregularities, we use three different indices which are described in (LEE, 2001). The first index evaluates the roundness of a dimensional shape by the following equation:

$$\frac{P^2}{4\pi A},$$

where P is the perimeter of the shape and A the area. This index will always be greater than 1 because the most compact dimensional shape is a circle. When calculating this index for a circle the result will always be 1 and this can be easily demonstrated by replacing P by the formula for the circumference of a circle and A by the formula for the area of a circle. The greater the value of this index, the greater is the border irregularity of the evaluated shape.

Lesions with irregular shape have a great variance in the distance between its centroid and its border (LEE, 2001). Based on this, the second index we use is the difference between maximum and minimum distances from the border of the lesion to its centroid. The index that relates the distance between centroid and border described in (LEE, 2001) calculates the variance of the distance from all points over the border to the centroid. However, for simplicity, we just use the difference between maximum and minimum distances. In addition, we normalize this index by dividing it by the minimum distance from the border to the centroid.

The third index we use to evaluate the irregularity of a lesion border relates the perimeter of the lesion and the perimeter of the convex hull of the lesion. We compute this index by using

$$\frac{P}{P_c},$$

where P is the perimeter of the lesion and P_c is the perimeter of the convex hull of the lesion.

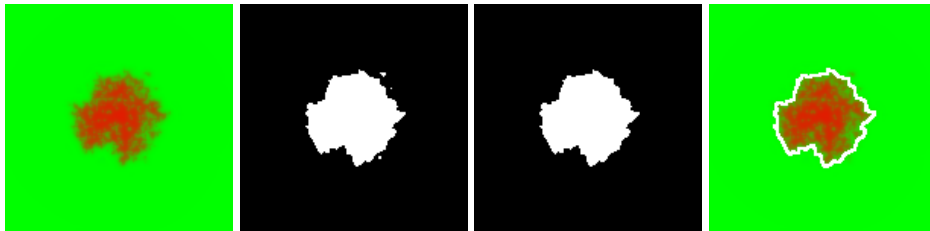### 4.5.1 Lesions and Results Segmentation

Figure 4.5: Segmentation of simulation results. Respectively we have: a visualization of the simulation result where green represents the healthy skin melanosomes concentration and red represents a high concentration of melanosomes; the segmentation result by using the threshold; a selected segmented area from the previous segmentation result; and a comparison between the selected area border and the simulation result.

Before we compute the indices used in the comparison between real lesions and simulation outputs, we have to separate lesions from healthy skin in real images and regions representing lesions from regions with normal melanosomes concentration in our simulation results. Regarding our simulation results, the segmentation is done by using thresholds in the concentration of melanosomes. Every region with a melanosomes concentration higher than a specified threshold will be a hyperpigmented lesion region. All

the regions with melanosomes concentration below a specified threshold will be a hypo-pigmented lesion region. The other regions with melanosomes concentration in between these thresholds represent healthy skin. In Figure 4.5 we have the segmentation result from this approach in a region with high concentration of melanosomes.

The segmentation of skin lesions is not a simple process and there are several approaches to this kind of segmentation. Basically, every work regarding the evaluation of pigmented lesions describes a different segmentation method. We decide to use a segmentation based on the Chan-Vese algorithm. We start with a real image of the lesion and a marker image that indicate some points inside the lesion. This marker image is made manually. Since we know that there is just one lesion in each lesion image, we remove all small connected regions of the Chan-Vese algorithm output. We also know that we do not have healthy skin regions inside a lesion. Thus, we fill the nonsegmented regions inside a segmented region. However, at this point, the segmentation result presents a very sharp border because of the slightly differences between the healthy skin color and the lesion border color. Thus, to improve the segmentation result, we dilate this sharp border and incorporate it to the segmentation. We do this dilation in the border by using the range filter and after this we add the range filter result to the segmentation reducing the border sharpness. Figure 4.6 illustrates the steps of the segmentation process.
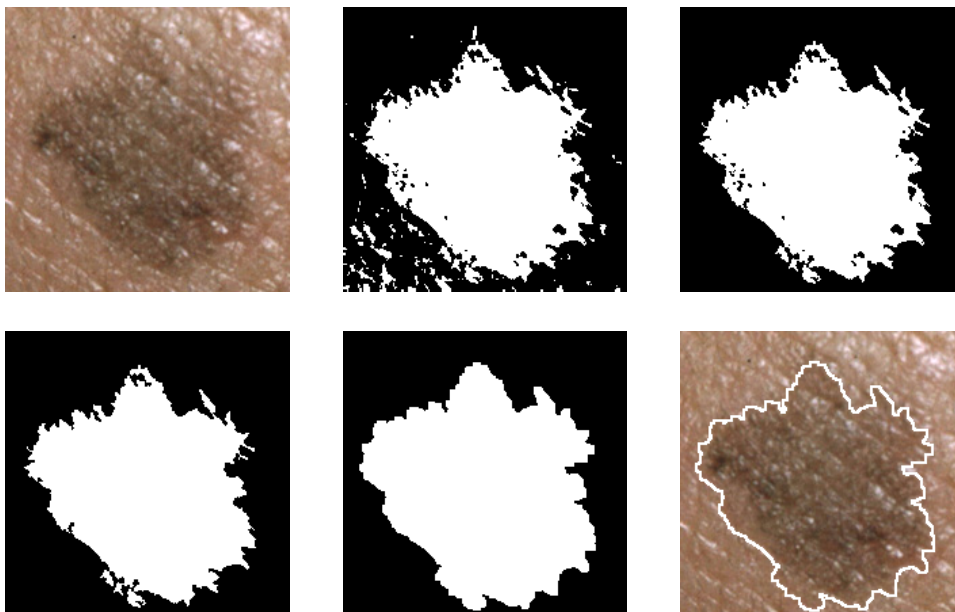

Figure 4.6: Pigmented lesions segmentation steps. We have, respectively: the input image, the Chan-Vese algorithm output, the result of removing the segmented regions outside the lesion, the result of filling the nonsegmented regions inside the lesion, the result of adding the range filter result to the segmentation, and an image to help the evaluation of segmentation quality.

4.5.2 Validation Results

In this validation, we just analyze clinical images of lentigines. We do that because we do not have access to good quality images of the other simulated pigmentation disorders. During the analysis of the lentigines clinical images, we discarded: images that present hair and other artifacts over the lesion, underexposed and overexposed images,

images with low resolution, and images where the skin surface was not aligned with the image plane so we avoid that the perspective distortion interfere in the collected data. We analyzed 31 clinical images of lentigines from dermatological repositories (DERMIS, 2013), (NEW ZEALAND DERMATOLOGICAL SOCIETY INCORPORATED, 2013), (SILVA; CALHEIROS, 2013), (USATINE, 2009), (VERROS, 2013), (EASTER et al., 2013), and from our own clinical studies. To compare with the clinical images of lentigines, we simulate 31 hyperpigmented lesions. We start the simulation setting 0.1% of normal melanocytes as melanocytes that reproduce faster in the central grid element. We simulate the growth of a lesion from this grid element. Also, D_f was defined in a way that around half of the cells present random diffusion coefficients uniformly distributed between 0 and 0.000002 and the other half between 0 and 0.0002.

As described previously, we analyze the asymmetry on both symmetry axes which was computed by using principal components decomposition. The axis with greater variance was aligned with the horizontal direction. Accordingly, we calculate the asymmetry in the horizontal and vertical axis. In Figure 4.7 we show the mean and standard deviation of horizontal and vertical asymmetry from the real lesion images and from the simulation results. The higher the computed asymmetry value, the greater is the lesion shape asymmetry.
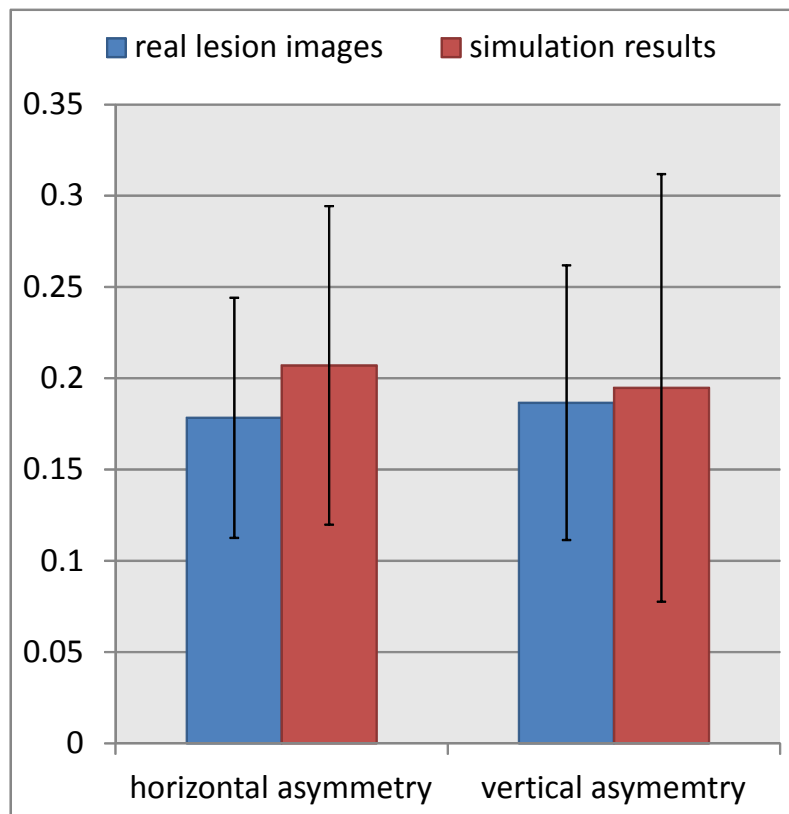

Figure 4.7: Lesions asymmetry.

As we can see in Figure 4.7 and in Table 4.2, our results are slightly more asymmetric than evaluated pigmented lesions. We believe this occurs because our system is able to produce not only lesions with characteristics of a lentigo but also lesions that resemble a melanoma and the melanomas have a more asymmetric shape. In addition, as we

know, lentigines are more symmetric if compared with melanomas. Thus, the comparison involving lentigines with our simulation results, which may include melanomas, results in this small difference in the asymmetry. This is enforced by the fact that the standard deviation of the simulation results is greater than the standard deviation of the analyzed lentigines. And accordingly, we have more variation in the simulation results that in the evaluated lesions which are a subset of the hyperpigmented skin lesions.

Regarding the border irregularity, we present the collected data from pigmented lesions in Figure 4.8. In this figure we can see the irregularity of the border measured by evaluating: the roundness of the lesion, named roundness index; the maximum and minimum distance from the border to the centroid of the lesion, named centroid index; and the relation between the lesion perimeter and its convex hull perimeter which is named convex hull index. The perimeter of the lesions was defined as the perimeter of the polygon formed by the center of the pixels, in real images, or by the center of the grid elements, in simulation results, that are located in the border of the lesion. In Figure 4.8 we show the mean values for these three indices from real lesions and from the simulated lesions. The black mark over the bars in the chart represents the standard deviation of the indices. Similarly, as the asymmetry value, the greater the value of these three indices, the greater is the border lesion irregularity.
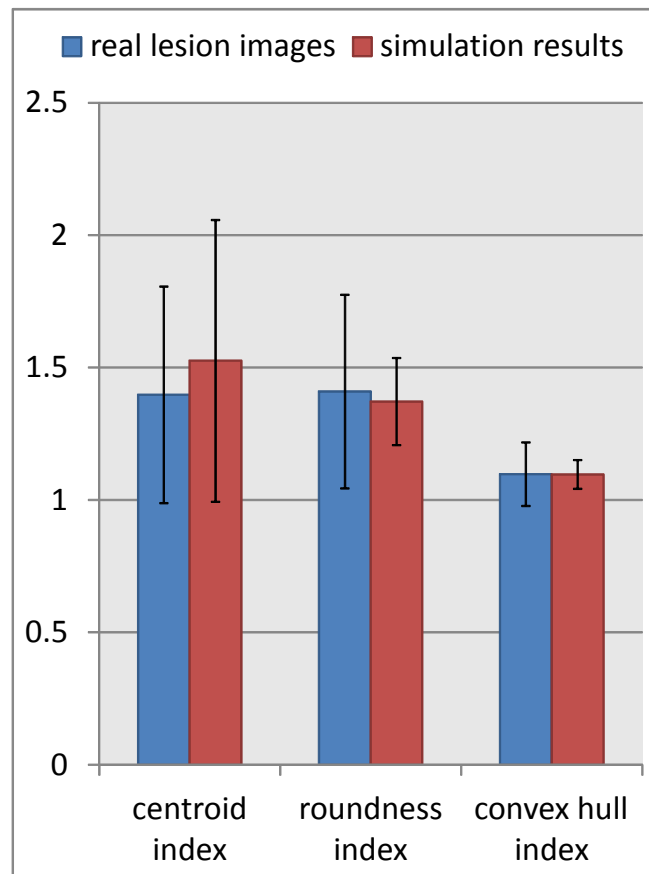

Figure 4.8: Lesions border irregularity.

In Figure 4.8 and Table 4.2 we can observe that there is virtually no difference between the simulation results and the real lesion images regarding the values of the convex

hull index. Also, we can note that the roundness index values of the simulation results are consistent with the values observed in real lesions. However, regarding the centroid index, we can see a more significant difference between the simulation results and the real lesions. A possible cause to this difference is the fact that this measure is unstable because the centroid position is very sensitive to small variation in the lesion border (LEE, 2001). Also, this index can indicate a very irregular border in a lesion which has an elliptical shape far from a circular shape regardless its border regularity.

	real lesion images		simulation results	
	μ	σ	μ	σ
horinzontal asymmetry	0,178370	0,065872	0,207115	0,087192
vertical asymmetry	0,186716	0,075258	0,194770	0,117149
centroid index	1,397410	0,409259	1,525728	0,532364
roundness index	1,409758	0,365335	1,371793	0,164604
convex hull index	1,096964	0,120108	1,095917	0,054630

Table 4.2: Validation results.

In order to help in understanding how the values in Table 4.2 are expressed in the lesions shape, in Figure 4.9, we show the segmentation of the simulated lesions with the highest and lowest values for all evaluated index. Despite being the index with highest standard deviation, we can note that the visual differences in the border irregularities between the lesions with maximum and minimum centroid index are subtle. We can also note in Figure 4.9 that we have the same lesions shape for the roundness and convex hull indices. This happens because both indices are calculated using the perimeter of the lesion shape.
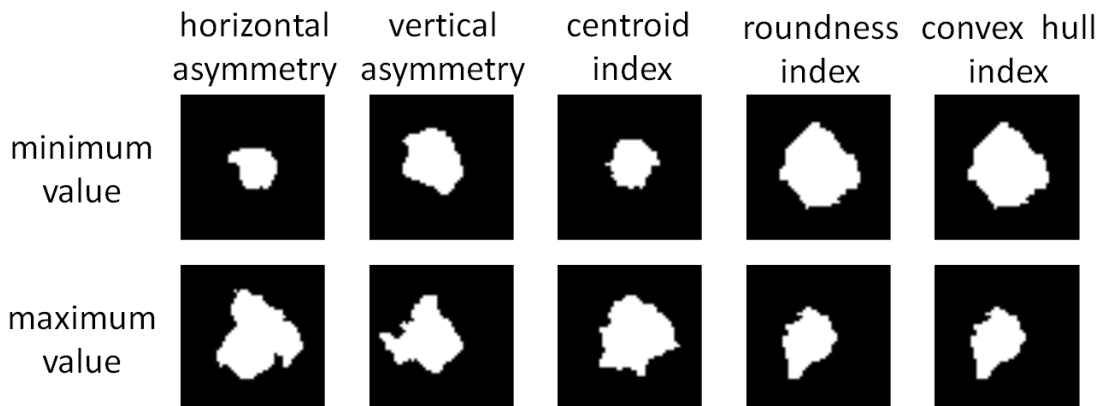
Figure 4.9: Shape of the simulated lesions with the highest and lowest values for all the indices used in the validation process.

As described in the previous section, we can control several characteristics of the simulated lesions. Thus, our system is able to produce lesions with different desired characteristics just by appropriately setting some parameters such as the diffusion functions. However, in order to have a more precise evaluation of our system, we decide to configure the system to produce lesions more similar with the evaluated real lesions which are lentigines.

Finally, we have to point out that the values of this comparison are strongly dependent of the segmentation process used since the segmentation results are the input to the computation of all measures described in this section. However, the development of skin lesion segmentation processes is still an explored topic in the dermatology. Since we used a segmentation based on generic segmentation algorithms, it may be possible to increase the quality of the validation by using a better segmentation process.

4.6 Other Models

Although simpler methods to generate pigmented lesions are possible, they do not capture main characteristics of real pigmented lesions. In order to compare our results we experimented with a naive cellular-automata diffusion model as presented in (BANDMAN, 1999) and then we apply a blurring to the output of this model. The spots generated by this approach show either little variation in color or ill-defined borders. In addition, the quality of the results of the cellular-automata approach strongly depends on the initial states of their cells. Thus, in order to generate good results it is necessary to develop an automated way to set these initial states.

We also try to generate pigmented lesions by doing a simple modification in the classical reaction-diffusion system proposed by Turing (TURING, 1952). This system consists of the following set of equations, where a is the activator and b is the inhibitor:

$$\frac{\partial a}{\partial t} = c(ab - a - \beta) + D_a \nabla^2 a \text{ and } \frac{\partial b}{\partial t} = c(16 - ab) + D_b \nabla^2 b.$$

Since some pigmented lesions have more irregular borders than the spots generated by the original Turing's system, we modified the activator's equation in order to reproduce this behavior to:

$$\frac{\partial a}{\partial t} = c(ab^2 - a - b - \beta) + D_a \nabla^2 a.$$

This modified system does not attempt to simulate the melanocytes and melanosomes dynamics. Thus, it only tries to reproduce the visual results that the melanocytes and melanosomes interactions cause in the skin.

In the Turing set of equations the β values have a small random variation from cell to cell and are sources of slight irregularities necessary for the dynamics of the system. These results look different for each set of β values but have the same overall pattern. We maintain β fixed for all cells in the grid and this allows more control in the simulation result. In our system, the different simulation results are obtained modifying the initial random distributions of the concentrations of a and b. An age spot is generated in a region where the initial b concentration is greater than the nearby initial a concentration. Thus, we can control the size and positioning of the age spots in the simulation result by manually setting these initial concentrations. Even this modified version of the Turing's system being more elaborated, it presents several difficulties regarding the control of the lesion features. In this approach, we have no way of specify or control major features of the pigmented lesions such as its border irregularities. We also cannot see the time evolution of a pigmented lesion by using this system.

Because this both simple approaches are not based on biological data, it is difficult to map the their outputs into a consistent skin color since the values contained in these outputs do not represents any biological data such as the melanosomes concentration. Thus we do not have a starting point to elaborate a method to convert the values of these
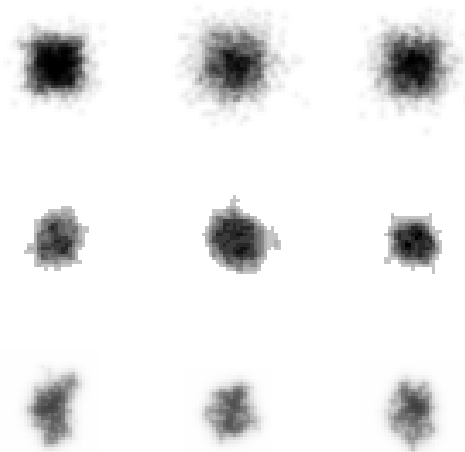
Figure 4.10: Visual comparison of other possible approaches to generating pigmented lesions. In the top row we have three spots generated by blurring the output of the naive cellular-automata diffusion model from (BANDMAN, 1999). In the middle row we have three isolated spots obtained from the modified reaction-diffusion system proposed by Turing. For comparison, in the bottom row we have three isolated hyperpigmented lesions from our reaction-diffusion system.

outputs into a consistent skin color or skin lesion color. It is possible to visualize the results of these both methods in Figure 4.10. In addition, for comparison purposes, we also include isolated pigmented lesions generated by our simulation model in Figure 4.10.

4.7 Summary

In this chapter we presented the main contribution of this work which is a reaction-diffusion system that models the generation and evolution of human skin pigmented lesions. Thus, we described how our system is related with the biological processes behind the pigmented lesions and, in this sense, we explained what is the biological role of each term of the differential equations and its influence in the system as a whole. Also, we described the biological assumptions that we made aiming to fill the knowledge gap regarding these processes.

Further, we described the initial conditions used to solve this system and we presented the different results we can produce by changing these initial conditions and other parameters of the simulation. Thus, aiming to evaluate the quality of these results, we also presented a comparison between real and simulated pigmented lesions. This comparison required the use a segmentation method to isolate the pigmented lesions and also required the definition of measures which were collected from the segmentation results. The collected information from real and simulated lesions was analyzed and we observed that the simulation results have characteristics which are consistent with the real lesion characteristics. Finally in this chapter, we discussed simpler and alternative methods to try to reproduce results similar to the final results of our system.

5 SIMULATION MODEL IN COMPUTER GRAPHICS

As mentioned in Chapter 1, we focus in the applications of our system related to computer graphics. Thus, in this chapter we describe how we use the simulation results of our model in computer graphics. Accordingly, we describe how to transfer the simulation output of our model to skin textures and exposed skin areas in pictures. First, in Section 5.1 we show an overview of the method used to realize this transfer. After that, we detail all the steps of this method. Thus, in Section 5.2, we describe how to map the size of a simulation result to the scale of the skin texture or picture. Later, in Section 5.3, we present a method to convert the computed melanosomes concentration into a skin color that is consistent with the skin color in the texture or picture where the simulation result will be transferred. However, before mapping the melanosomes concentration into colors, we have to deal with the perspective distortion presented in these photos. Thus, we present the method used to treat this perspective distortion in Section 5.4. We show our final results in Section 5.5.

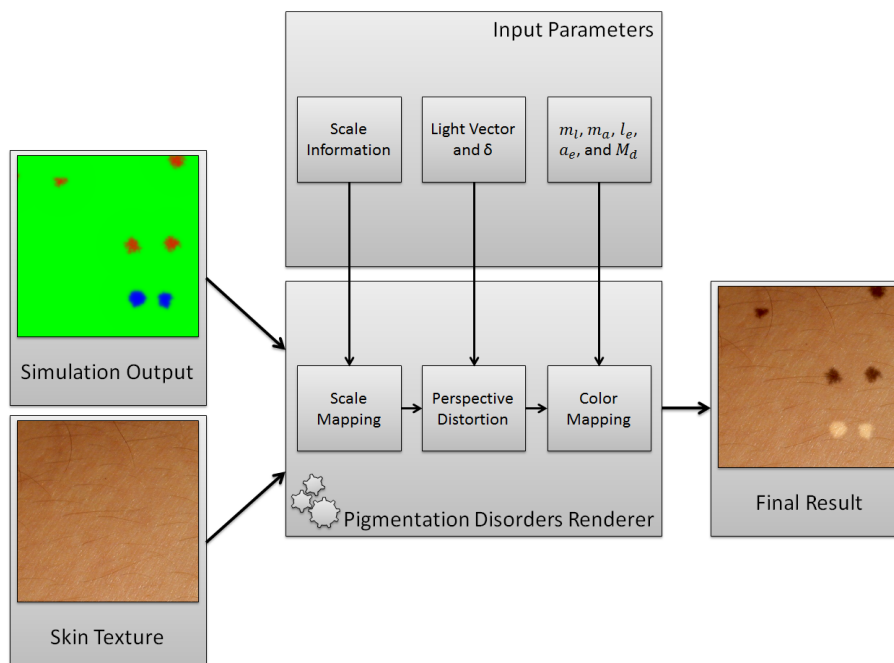## 5.1 Pigmentation Disorders Renderer Overview

Figure 5.1: Pigmentation disorders renderer overview.

The process of mapping the melanosomes concentration calculated by the simulation model into a pigmented lesion rendered in a skin image is divided in three main steps: scale mapping, perspective distortion treatment, and color mapping. Figure 5.1 illustrate this process.

The first step assigns a melanosomes concentration value to every pixel in the skin image where the pigmented lesions will be rendered. This first step has to maintain a consistent concentration of melanosomes despite the differences in scale between the simulation output and the skin image. After that, we treat the existing perspective distortion in this skin image and we assign new texture coordinates to every pixel in this image which will rearrange the melanosomes concentration for every pixel in the skin image. Finally, the melanosomes concentration associated to a pixel in the skin image is used to calculate the new color of this pixel.

The simulation results rendering process obviously depends on the output of the pigmented lesions simulation model which is well detailed in Chapter 4. As we focus on the applications of our model in computer graphics, we had to develop this pigmentation disorders renderer that together with the simulation model forms a complete system to generate and render human pigmentation disorders. The overall system organization is presented in Figure 5.2. Both main parts of this system are configured with several input parameters. Most of these parameters has default values which minimizes the effort to configure a simulation. The final output of this system will be a skin image with synthesized pigmented lesions or also a skin texture with synthesizes pigmented lesions able to be applied in a human model.
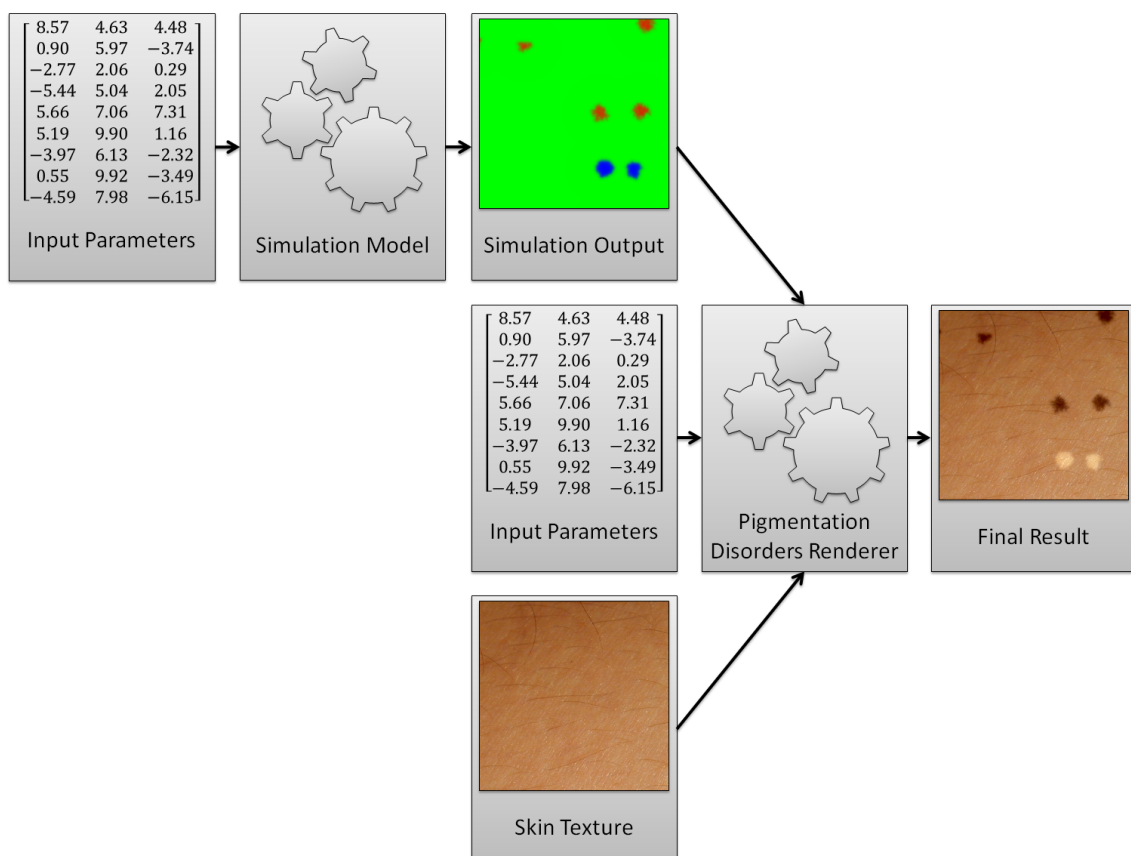

Figure 5.2: Complete rendering process of the pigmented skin lesions.

5.2 Mapping the Scale of the Simulation Results

As described in Chapter 4, each grid element in the simulation starts with 10 normal melanocytes. Also, accordingly with the data presented in (BURNS et al., 2010), we can estimate how many grid elements are needed to represent a squared millimeter of skin keeping the concentration of 10 normal melanocytes by grid element. As illustrated in Figure 3.4, this concentration varies from a body region to another therefore, respecting this variation, we calculate that one square millimeter can be represented by a squared patch with a side measuring from 12 up to 16 grid elements.

In order to compute how many grid elements have to be used to represent a squared millimeter of skin, we have to know where in the body is located the skin texture or picture that will receive the simulation result. Once we know the region of the body, we use the concentration of normal melanocytes in this region accordingly to (BURNS et al., 2010) and calculate the number of grid elements in a squared millimeter of skin. When we do not know the region of the body, we use the intermediate value of 14x14 grid elements to represent a squared millimeter of skin.

After defining the number of grid elements of the simulation that are necessary to represent a squared millimeter of skin, we have to compute how many pixels are used to represent a squared millimeter in the texture or picture where the simulation results will be applied. Basically, we use the provided scale information to discover the amount of pixels used to form a millimeter. After that, we use bilinear interpolation to calculate the melanosomes concentration for every pixel based on the melanosome concentrations of the grid elements from the simulation output. Figure 5.3 illustrates this process.
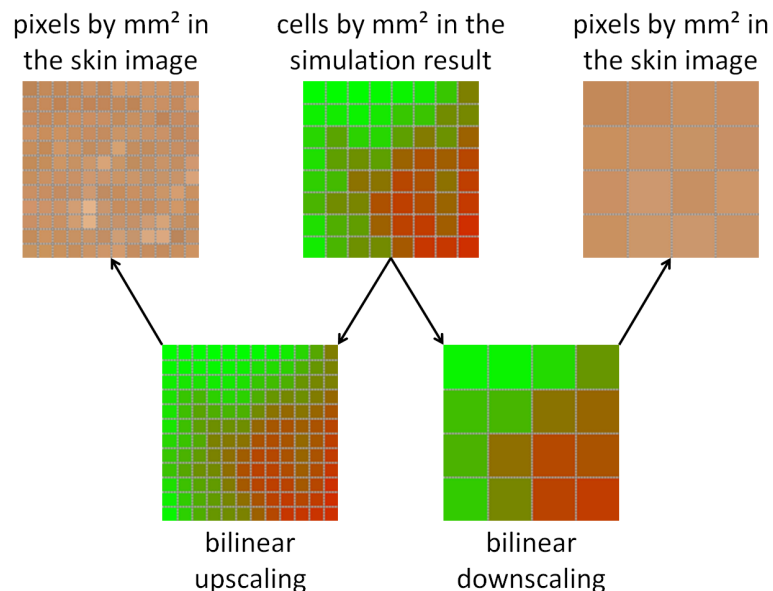
Figure 5.3: Mapping the size of the system output to the skin image scale.

Very few dermatological images present scale information. Thus, in images without this information the amount of pixels that represents a squared millimeter is set manually until a visually satisfactory result is produced. This approach is also used in images that present perspective distortion so the number of pixels used to represent a millimeter changes accordingly to this distortion.

After mapping the scale of the simulation results, we have a melanosomes concentration associated with every pixel. This melanosomes concentration will be used to change the original pixel color in way that the pixel color will reflect the new melanosomes concentration applied in the skin region represented by this pixel. This process of mapping a melanosomes concentration value into a consistent skin color will be explained in the next section.

5.3   Mapping the Melanosomes Concentration into a Color

All the computations regarding the color of pigmented lesion are done by using the L*a*b* color space. In dermatology context, L*a*b*is probably the most used color system. Also, it is the standard for colorimeter in industry and most of the commercially available reflectance devices display L*a*b* values (TAKIWAKI et al., 2002). In this color space, L* represents the color lightness where 0 means black and 100 indicates diffuse white; a* determines the green-red chromaticity where negative values indicate green and positive values indicate red; and b* determines the blue-yellow chromaticity where negative values indicate blue and positive values indicate yellow. Figure 5.4 illustrates the three coordinates of the L*a*b* color space.
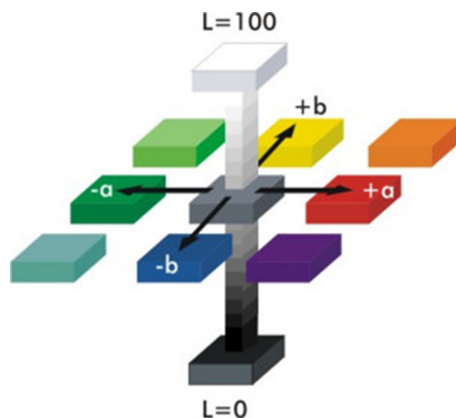

Figure 5.4: L*a*b* color space.

According to (TAKIWAKI et al., 2002), we know that the variation of melanin in the skin implies in the variation of the L* and a* components of the skin color. More specifically, when the amount of melanin decreases in the skin its color has the L* component increased and the a* component decreased. On the other hand, when the amount of melanin increases then the L* component decreases and the a* component increases. In Figure 5.5 we can see the effect of increased and decreased melanin concentration in a skin color sample simulated through the variation of L* and a* components.

Since we know that the melanin concentration variation implies in the variation of the L* and a* components of the skin color, and we know that the melanin is located inside the melanosomes, we determine the resulting color of a pigmented lesion based on the melanosomes concentration computed in our model, and in the original skin color of the region where this pigmented lesion will be rendered. The output of our model may represent one of three different situations: when the melanosomes concentration is normal and no lesion have to be rendered; when the melanosomes concentration is greater than normal and a hyperpigmented lesion have to be rendered; and when the

melanosomes concentration is less than normal and a hypopigmented lesion have to be rendered. Obviously, when no lesion has to be rendered we maintain the original skin color. Thus, in the regions with normal melanosomes concentration we do not compute a different skin color because there is no melanin concentration variation and consequently no skin color variation.
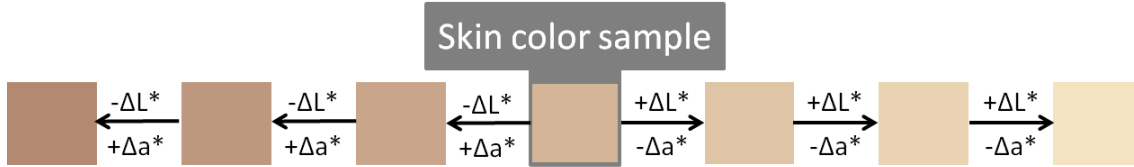

Figure 5.5: Simulation of skin color variation due to melanin concentration changes by altering the L* and a* components of the original skin color, where $\Delta L^* = 5$ and $\Delta a^* = 2$.

In order to compute the color of a region with melanosomes concentration different from normal we use:

$$r_l = o_l + (m_l - o_l)(M_n)^{l_e} \text{ and } r_a = o_a + (m_a - o_a)(M_n)^{a_e},$$

where o_l and o_a represent respectively the L* and a* components of the original skin color of a region with normal melanosomes concentration and r_l and r_a represents respectively the resulting L* and a* of the color corresponding to the melanosomes concentration calculated in our simulation model and represented by M_n. This melanosomes concentration is normalized in a way that in regions of the simulation output with melanosomes concentration above normal we have

$$M_n = \frac{M - M_d}{M_{max} - M_d},$$

where M is the melanosomes concentration computed our simulation, M_d is the default melanosomes concentration which is the concentration found in normal and healthy skin regions, and M_{max} is the maximum melanosomes concentration found in the simulation output. Also, in regions with melanosomes concentration below normal we have

$$M_n = \frac{-(M - M_d)}{M_d}.$$

m_l and m_a represent the maximum variation in L* and a* respectively.

When computing the resulting color of a region with melanosomes concentration above normal m_a will be a positive value and m_l a negative value. Accordingly, in a region with melanosomes concentration below normal, m_l will be a positive value and m_a a negative value. Table 5.1 shows the default values of the parameters used to find a resulting skin color based on the melanosomes concentration calculated in our simulation model. All the values in Table 5.1 were defined accordingly with the values described in (TAKIWAKI et al., 2002) and also according to color measurements realized in our pigmented lesions database. However, these values may be changed to achieve a specific result. For instance, if we set values for l_e and l_a different from 1 we will obtain a non-linear mapping from a melanosomes concentration into a resulting color. The different results obtained by the variation of l_e and l_a values are illustrated in Figure 5.6.
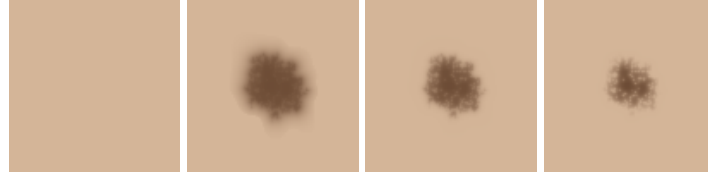
Figure 5.6: l_e and l_a variation. From left to right: an image with a solid sample skin color, and color mapping results with l_e and l_a equals to 0.3, 1 and 3 respectively.

In this approach we just change the L* and a* components of a skin texture or image according to the computed melanosomes concentration. Despite being a simple method, this approach is able to produce visually consistent results which also preserve the original illumination conditions because we just reproduce the skin color variation through a slight increasing or decreasing in the original L* and a* components values. Further, the alteration of these components values is consistent with real collected data and the L*a*b* color space was designed in way that uniform changes in its components reflect the uniform changes in the perceived color. In short, we do not consider or evaluate individual colors but just the variations of a healthy skin color according to the melanin variation in the Lab color space.

| | when the melanosomes concentration is | |
parameter	greater than normal	less than normal
m_l	-40	20
m_a	4	-8
l_e	1	1
a_e	1	1
M_d	60	60

Table 5.1: Default values of the color mapping parameters.

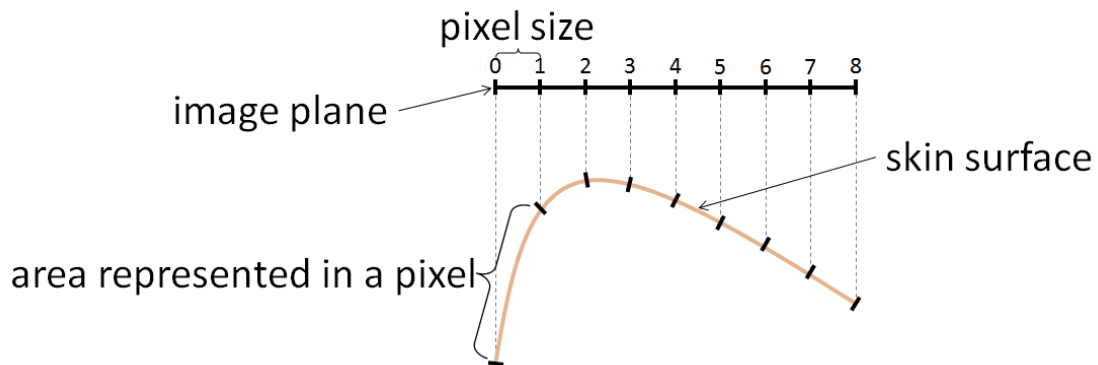## 5.4 Treating the Perspective Distortion

Figure 5.7: An illustration of a scenario with perspective distortion.

Sometimes, the skin surface captured in an image is non-orthogonal to the viewer. In this scenario, illustrated in Figure 5.7, there are perspective distortions which cause the

pixels to represent different area sizes in the captured skin surface. Thus, it is not possible to change a pixel color accordingly with the melanosomes concentration value associated to this pixel because the skin surface area represented by the pixel and the area associated with the concentration value are different. Thus, we need to treat the simulation result after the scale corrections and before the color mapping process to correct these area inconsistences. Originally, the texture coordinates of every pixel are its own coordinates. However, to correct the perspective distortion, we have to calculate new texture coordinates $\mathbf{t} = (x + u, y + v)$ for each pixel $\mathbf{p} = (x, y)$. Figure 5.8 illustrates the new texture coordinates of the pixels illustrated in Figure 5.7.
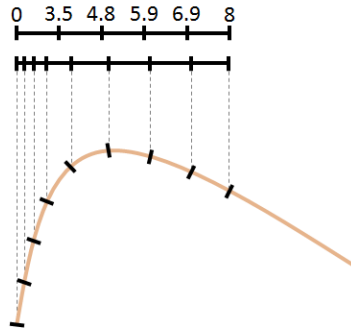

Figure 5.8: An illustration of a scenario where the perspective distortion was treated.

Before treating the perspective distortion we have to extract any feature from the skin image that makes possible to represent the skin surface geometry. (WINNEMÖLLER et al., 2009) and (FANG; HART, 2004) try to estimate the surface geometry by recovering the surface normals. Thus, based on this works and in our observations we find that only the skin surface normals are sufficient to treat the perspective distortion. Below, we present the method used to estimate the skin surface normals from a skin picture.

5.4.1 Normal Recovery

According to (FANG; HART, 2004), we find that the simple Lambertian reflectance model works well to recover the skin surface normals. To recover the skin surface normals we use the luminance information contained in the L* image channel. We also need the vector indicating the direction of light that reaches the skin. We can manually specify this vector but if not we consider the vector coming from the camera position and orthogonal to the image plane. Differently from (FANG; HART, 2004), to avoid noise in the recovered normals, we applied a Gaussian smoothing in the L* channel of the image before recovering the normals.

In this way, first we normalize all the L* values so that they fall in between 0 and 1, where 0 and 1 represent the minimum and the maximum L* values respectively and $\mathbf{i}(x, y)$ represents this normalized light intensity at the pixel with x and y coordinates. Also, we need a three dimensional vector with components that are the image gradient in the x direction, the image gradient in the y direction, and 0. This three dimensional vector is represented by $\mathbf{g}(x, y)$ and the gradients in its components are calculated at pixel with coordinates x and y. Then, $\mathbf{l}$ being a unit vector that points to the light source, we can calculate the normal vector at the pixel with x and y coordinates, which is represented by $\mathbf{n}(x, y)$, using the following equation:

$$\mathbf{n}(x,y) = \mathbf{l}\,\mathbf{i}(x,y) + \frac{(\sqrt{1-(\mathbf{i}(x,y))^2})(\mathbf{g}(x,y)\cdot\mathbf{l})}{\|\mathbf{g}(x,y)\cdot\mathbf{l}\|},$$

which is presented in (FANG; HART, 2004).

As mentioned previously, the vector which indicates the light direction can be manually set. Based on this vector we calculate $\mathbf{l}$ which is a unit vector in the opposite direction of the manually set vector. By default, we use $\mathbf{l} = (0,0,1)$. Also, we need to point out that the approach used to capture the normals of the skin surface is not very accurate. However, it is able to describe the skin surface geometry in a manner that is adequate to our purposes.

5.4.2 Texture Distortion

To achieve the illusion that the pigmented lesions follows the skin surface we need to calculate a new texture coordinate for each pixel based on the recovered normal at this pixel. Thus, considering $\mathbf{n}'$ as the normal of a surface which is parallel to the image plane, we know that there is no distortion when the skin surface is equal to $\mathbf{n}'$. In this case, the normal of this surface takes the form $(0,0,n_z)$. We also know that the closer to $90°$ the angle between $\mathbf{n}'$ and the normal recovered at an arbitrary pixel, the greater the perspective distortion.

Figure 5.9: Plots of the functions which calculate the vertical texture coordinate (in blue) and its second derivative (in magenta).

All the normals which we have to deal are present in a hemisphere since we only have to deal with the normals of the visible skin surfaces. Thus, we start with the equations that calculate the texture coordinates of a hemisphere whose radius is equal to 1. We use this value for the hemisphere radius because in this way the spatial coordinates of a point on the hemisphere surface represent the normalized components of the normal at this

point. These equations associate each point in a texture with a point over the hemisphere surface. However, we do not want to make this association but calculate the distortion of the texture coordinate in every point over the hemisphere surface. As these points have an associated normal, we can calculate the texture coordinate distortion for every normal in this hemisphere by knowing the distortion for every point on the hemisphere surface.

We find that the second derivative of the equations which calculates the texture coordinates for this hemisphere approximates the distortion effect we want to reproduce. In 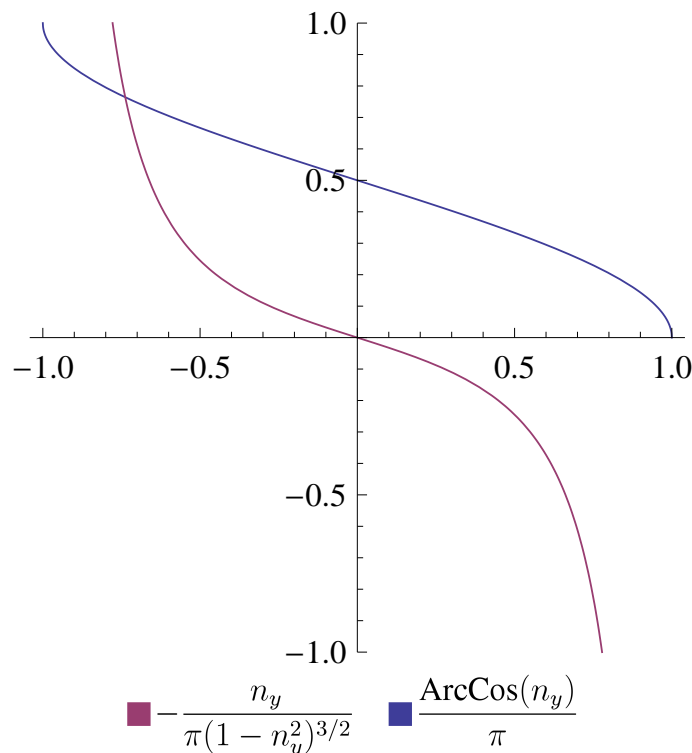Figure 5.9, we plotted the function which calculate the vertical texture coordinate (in blue) and its second derivative (in magenta), where n_y represents the y coordinate of the point in the hemisphere surface and also the y component of the normal vector at this point. As we can see in Figure 5.9, the second derivative determines no distortion (vertical axis) when the n_y value (horizontal axis) is equal to 0. Also, the distortion increases as the normal nears the $(0, -1, 0)$ and $(0, 1, 0)$ which forms a 90° angle with $\mathbf{n}'$. Thus, we can see that the second derivative of the hemisphere texture coordinate equations have all the desired properties to reproduce the desired distortion effect.

Thus, considering that the image dimensions are normalized between 0 and 1, for each pixel $\mathbf{p} = (x, y)$ with the associated normal $\mathbf{n} = (n_x, n_y, n_z)$ we calculate its texture coordinate $\mathbf{t} = (x + u, y + v)$ where

$$v = -\frac{\delta n_y}{\pi(1 - n_y^2)^{3/2}}, \, u = \frac{\delta n_x \text{CosSec}(\alpha\pi)^3}{\pi(1 - n_x^2 \text{CosSec}(\alpha\pi)^2)^{3/2}}, \text{ and } \alpha = \frac{\text{ArcCos}(n_y)}{\pi}.$$

The δ parameter was added to increase or decrease the distortion magnitude. The default distortion magnitude used is $\delta = 0.18$. In this approach, a wide region with the same normal will not present a distortion because we do not propagate the distortion of a pixel to the surrounding pixels. On the other hand, skin surface images do not have regions flat or inclined enough to notice this effect. In Figure 5.10 we can see the effect of distortion obtained by our approach.

Figure 5.10: A normal map and the distortion caused by this normal map.

(FANG; HART, 2004) present a technique to reproduce this kind of texture distortion. This technique create pixels patches by clustering the normals associated to these pixels and then calculate new texture coordinates for these pixels in accordance with a normal associated with the patch. There are inconsistencies that increase in severity with the distance between a pixel in a patch and the centroid of this patch. The patches overlap each other and they are sewn through the overlapping areas by the graphcut algorithm. In this technique, it is possible that the shape of the pigmented lesions change in a way that they can no longer produce a realistic result. Also, (WINNEMÖLLER et al., 2009) uses

the parallax mapping to distort texture and suggests complex surface geometry in images. This technique simply deforms textures to give the impression of parallax foreshortening and it is not able to reproduce the perspective distortion effect we desire. In addition, this technique also requires the computation of a height-field from the recovered surface normals. Thus, because of the limitations of these both approaches, we had to develop another way to reproduce the perspective distortion effect in our results.

5.5 Results

In this section we show our simulation results. We can see samples of results from the pigmentation disorders simulation model proposed in this work in Figure 5.11. The lesions shown in this figure were mapped to a healthy skin picture. All these lesions were generated by using the default values for the input parameters except by the hyperpigmented lesions where the used values for l_e and l_a were 0.3. We also define manually the grid element where a portion of normal melanocytes suffers mutations. We do this in order to determine the location from where the pigmented lesions begin to develop. To control the size of these lesions we use the number of time steps of the simulation. For the hyperpigmented lesions we use 800 time steps and for the hypopigmented lesions we use 300 time steps. Each lesion was simulated in a grid of 100×100 grid elements and the time used to process this simulation was approximately 10 seconds for the hyperpigmented lesions and 5 seconds for the hypopigmented lesions. In Figure 5.11, we also present clinical images from hyperpigmented and hypopigmented lesions for comparison purposes. In addition, as we can observe in Figure 5.11, the the synthesized lesions are similar in shape, color and size with the real lesions.
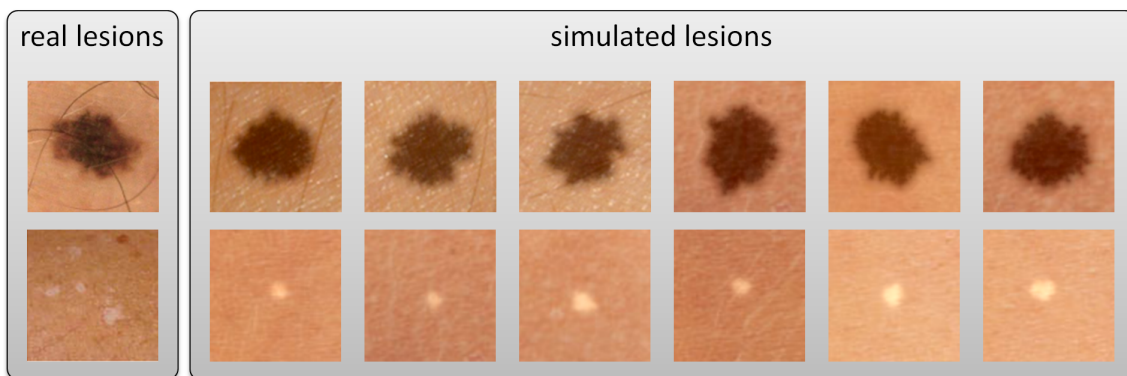

Figure 5.11: Examples of hyperpigmented and hypopigmented lesions generated by our system.

Also in order to evaluate our results, we used real before-and-after images of cosmetic procedures on patients with hyperpigmented skin lesions in Figure 5.12, and we map our simulation results to the images after the cosmetic procedure which removes the hyperpigmented lesions. Thus, in the first column of Figure 5.12, we show images of individuals before the laser skin treatment for hyperpigmented lesions removal. The second column of Figure 5.12 shows the result of this treatment, and the third column show our simulation results mapped to the individuals image after this treatment. For produce the result shown in the first row of Figure 5.12 we change the default values of m_l, l_e, and a_e to -15, 0.4, and 0.4 respectively. For the result in the second row we use $G_f = 0.2$, $m_l = -17.5$, $l_e = 0.4$, $a_e = 0.4$, and the other parameters were set with their default values. Finally,

for the result in the third row of Figure 5.12 we $m_l = -15$, and the default values for the other input parameters.

Figure 5.12: Comparing real pigmented lesions with the lesions synthesized by our system. In the first column we have the images of skin regions before a treatment for pigmentation disorders removal, in the second column we have the treatment results, and in the third column we show hyperpigmented lesions synthesized by our system.

In Figure 5.13, we generate some results aiming to reproduce pigmented lesions with unusual characteristics. In first row of this figure, we have: a lesion with an ill-defined border, an IGH lesion with very asymmetric shape in an individual with dark skin, a very dark and asymmetric lentigo, and a lentigo in a very dry and pale skin. All hyperpigmented lesions was rendered by using l_e and a_e equal to 0.3 except the last result of the first column which use the l_e and a_e default values. The remaining parameters were set with their default values. In the results shown in Figure 5.13, we can observe that our system can reproduce even pigmented lesions with unusual characteristics without requiring a careful adjustment of its parameters.
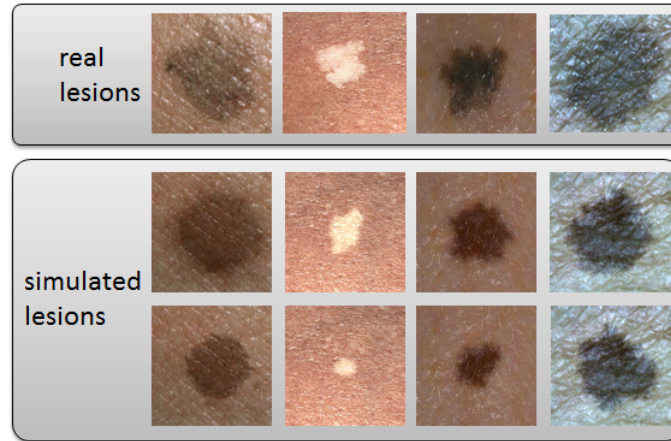
Figure 5.13: Results aiming to reproduce unusual pigmented skin lesions.

5.6 Summary

In this chapter we presented the process used to convert the output of our simulation model into synthetic human pigmented lesion pictures. This process can also be used to add the artifacts from pigmentation disorders in skin textures of virtual human models. This process is formed by three steps and each step deals with a specific problem.

First, we deal with the differences involving the scale of the simulation computations and the skin image scale. After that, we deal with the perspective distortion that may occur when the skin surface represented in the skin image is not aligned with the skin image plane. Finally, after assigning melanosomes concentration values to the skin image pixels, we compute the new color of this pixel considering its original color and the melanosomes concentration assigned to this pixel.

Also in this chapter, we described the overall structure of the system used to generate and render the human pigmentation disorders. We also presented and discussed the final results of this system. These results are also visually compared with real clinical images of pigmented lesions.

6 CONCLUSIONS AND FUTURE WORK

Our work presented a new model for simulation of human pigmentation disorders. Our model consists of a biologically inspired reaction-diffusion system which models the processes behind the melanocytes life cycle, its mutations and its melanosomes production. As far as we know, our work is the first that proposes a mathematical model to simulate these processes and their effects on the human pigmentary system. The parameters used in this system were derived from dermatological data or were defined in order to achieve a specific visual result. The reaction-diffusion was structured such that the parameters have a well defined output. Thus, the manual definition of some parameters of the system was a simple task because we know the effect of changing these parameters values and we know the result we want to reproduce.

Also, we measured the features of the pigmented lesions generated by our system and we compared these features with the features measured from real pigmented lesions. In this comparison, we can observe that the characteristics of the pigmented lesions synthesized in our model are consistent with the characteristics found in real pigmented lesions.

As we focus in the applications of our system in computer graphics, we also developed a method to map the simulation results to skin pictures or textures. This method deals with the scale, color and perspective distortions. We have to point out that the developed technique to calculate the final color of a pixel based on its associated melanosomes concentration was also inspired in biological information which is presented in (TAKIWAKI et al., 2002).

Thus, the main contributions of our work are: a model that simulates the interactions between the melanocytes and its melanin production, and a method to map the results of our simulation model to skin pictures and textures. In order to evaluate the quality of the output from our simulation model, we extract 5 measures from the shape of: the outputs of our simulation model and the segmentation results of real skin lesions images. After this extraction, we compare these measures and we find that the characteristics of our simulation results are consistent with the characteristics of real pigmented lesions. Also, in order to evaluate the method used to render the simulation output data producing a synthesized pigmented lesion image, we show real pigmented lesion images along with synthesized lesions images. Through these images, we can see that real and synthesized images are almost indistinguishable in shape and color.

Thus, we can conclude that the system formed by the simulation model and the pigmentation disorder renderer is able is able to synthesize the pigmentation disorders artifacts in healthy skin images. In computer graphics, this artifacts can be used to improve the realism of a skin texture, to help in procedural skin texture generation, and to improve the quality of human aging simulation since we know that pigmentation disorders are a more frequent in old people. Also, in our work, we show several information related to

the human skin which was presented in order to help in the understanding of the simulation model and the pigmentation disorders renderer. We believe that this information can be useful to any work regarding human skin in computer graphics since we present a rich description about the biological aspects of the human skin.

6.1 Future Work

The current time to run a simulation does not allow its use in real time applications. The required time to obtain a simulation result depends on the grid size and on the number of processed time steps. For example, a simulation with a 100×100 grid size and 800 time steps demands around 10 seconds by using a single thread in a 3.30 GHz CPU. A first obvious optimization consists in allowing the simulation to use more than just one thread. Also, we can use multigrid techniques and GPU processing to decrease this time. Thus, by decreasing the processing time of a simulation, we can be able to explore the usage of this model in real time applications. However, we must emphasize that the process of rendering a pigmented lesion is fast enough to be used in real time applications. Thus, the bottleneck in synthesized lesion image generation resides only in the simulation model.

Our model can be used not only in computer graphics. Thus, we still have to explore the features of our model in dermatology. Currently, our model is configured in such way that we produce results similar to clinical images of pigmented lesions. However, in dermatology, images from the underneath skin layers are also used to diagnosis purposes. In this sense, we believe that our model can also be used to generate this type of image. The possibility of use this model to such purpose aroused the interest of collaboration from researchers that deal with automated screening and diagnosis of hyperpigmented human skin lesions. Also, we believe that our model can be used in other dermatological contexts, for example, we believe that our model can be used to assist in the training of dermatologists about pigmentation disorders.

The proposed model was evaluated by comparing its results with real lesions using indices that quantify asymmetry and border irregularities. We just perform this evaluation using lentigines images. Thus, if we have access to more lesions images, images with higher quality, or more precise information regarding pigmented lesions, we can fine-tune our system in order to produce better results.

REFERENCES

ALBERT, A.; RICANEK JR, K.; PATTERSON, E. A review of the literature on the aging adult skull and face: implications for forensic science research and applications. **Forensic Science International**, [S.l.], v.172, n.1, p.1–9, 2007.

ALCÓN, J. et al. Automatic imaging system with decision support for inspection of pigmented skin lesions and melanoma diagnosis. **Selected Topics in Signal Processing, IEEE Journal of**, [S.l.], v.3, n.1, p.14–25, 2009.

BANDMAN, O. Comparative Study of Cellular-Automata Diffusion Models. In: MALYSHKIN, V. (Ed.). **Parallel Computing Technologies**. [S.l.]: Springer Berlin / Heidelberg, 1999. p.756–756. (Lecture Notes in Computer Science, v.1662).

BARANYI, J.; ROBERTS, T. A. A dynamic approach to predicting bacterial growth in food. **International journal of food microbiology**, [S.l.], v.23, n.3, p.277–294, 1994.

BARANYI, J.; ROBERTS, T.; MCCLURE, P. A non-autonomous differential equation to modelbacterial growth. **Food Microbiology**, [S.l.], v.10, n.1, p.43–59, 1993.

BARNHILL, R.; PIEPKORN, M.; BUSAM, K. **Pathology of Melanocytic Nevi and Malignant Melanoma**. [S.l.]: Springer, 2004.

BOISSIEUX, L. et al. Simulation of skin aging and wrinkles with cosmetics insight. In: COMPUTER ANIMATION AND SIMULATION. **Anais...** [S.l.: s.n.], 2000. p.15–27.

BURNS, T. et al. (Ed.). **Rook's Textbook of Dermatology**. 8.ed. [S.l.]: Wiley-Blackwell, 2010.

COTRAN, R. S. et al. **Robbins Pathologic Basis of Disease**. [S.l.]: Saunders, 1999.

DERMIS. **DermIS**. 2013.

DHAWAN, A. P.; SIM, A. Segmentation of images of skin lesions using color and texture information of surface pigmentation. **Computerized Medical Imaging and Graphics**, [S.l.], v.16, n.3, p.163–177, 1992.

DERMQUEST.COM. 2013.

EMRE CELEBI, M. et al. Border detection in dermoscopy images using statistical region merging. **Skin Research and Technology**, [S.l.], v.14, n.3, p.347–353, 2008.

FANG, H.; HART, J. C. Textureshop: texture synthesis as a photograph editing tool. **ACM Transactions on Graphics (TOG)**, [S.l.], v.23, n.3, p.354–359, 2004.

FERREIRA JR., S.; MARTINS, M.; VILELA, M. Reaction-diffusion model for the growth of avascular tumor. **Physical Review E**, [S.l.], v.65, n.2, 2002.

GANDHI, M. **A method for automatic synthesis of aged human facial images**. 2004. Tese (Doutorado em Ciência da Computação) — McGill University.

GATENBY, R. A.; GAWLINSKI, E. T. A reaction-diffusion model of cancer invasion. **Cancer Research**, [S.l.], v.56, n.24, p.5745–5753, 1996.

GOLOVINSKIY, A. et al. A statistical model for synthesis of detailed facial geometry. In: ACM TRANSACTIONS ON GRAPHICS (TOG). **Anais...** [S.l.: s.n.], 2006. v.25, n.3, p.1025–1034.

HUBBALL, D.; CHEN, M.; GRANT, P. Image-based Aging Using Evolutionary Computing. In: COMPUTER GRAPHICS FORUM. **Anais...** [S.l.: s.n.], 2008. v.27, n.2, p.607–616.

HUSSEIN, H. Towards realistic facial modeling and re-rendering of human skin aging animation. In: SHAPE MODELING INTERNATIONAL, 2002. PROCEEDINGS. **Anais...** [S.l.: s.n.], 2002. p.205–212.

IGARASHI, T.; NISHINO, K.; NAYAR, S. K. **The Appearance of Human Skin**. [S.l.]: Columbia University, 2005.

JIMÉNEZ, Z. A.; STEINBOCK, O. Stationary Vortex Loops Induced by Filament Interaction and Local Pinning in a Chemical Reaction-Diffusion System. **Physical Review Letters**, [S.l.], v.109, n.9, 2012.

KARDASHOV, V. et al. Nonlinear reaction-diffusion models of self-organization and deterministic chaos: theory and possible applications to description of electrical cardiac activity and cardiovascular circulation. **Discrete Dynamics in Nature and Society**, [S.l.], v.2006, 2006.

KASAI, S.; MORISHIMA, S. Aging model of human face by averaging geometry and filtering texture in database. In: SIGGRAPH'09: POSTERS. **Anais...** [S.l.: s.n.], 2009. p.61.

KHAIN, E.; SANDER, L. M. Dynamics and pattern formation in invasive tumor growth. **Physical review letters**, [S.l.], v.96, n.18, p.188103, 2006.

KIDER, J. T.; RAJA, S.; BADLER, N. I. Fruit Senescence and Decay Simulation. In: COMPUTER GRAPHICS FORUM. **Anais...** [S.l.: s.n.], 2011. v.30, n.2, p.257–266.

KONUKOGLU, E. et al. Image guided personalization of reaction-diffusion type tumor growth models using modified anisotropic eikonal equations. **Medical Imaging, IEEE Transactions on**, [S.l.], v.29, n.1, p.77–95, 2010.

LEE, T. K. **Measuring Border Irregularity and Shape of Cutaneous Melanocytic Lesions**. 2001. Tese (Doutorado em Ciência da Computação) — Simon Fraser University.

LIU, Z.; ZHANG, Z.; SHAN, Y. Image-based surface detail transfer. **Computer Graphics and Applications, IEEE**, [S.l.], v.24, n.3, p.30–35, 2004.

LUALDI, M. et al. Development of simulated pigmented lesions in an optical skin-tissue phantom: experimental measurements in the visible and near infrared. **Journal of Laser Applications**, [S.l.], v.14, p.122, 2002.

MAZZOLI, A.; MUNARETTO, R.; SCALISE, L. Development of optical tissue phantoms for the evaluation of the thickness of pigmented skin lesions by a conveniently purpose-modified digital camera: numerical simulations and experimental measures. In: SIXTH IASTED INTERNATIONAL CONFERENCE ON BIOMEDICAL ENGINEERING, Anaheim, CA, USA. **Proceedings...** ACTA Press, 2008. p.172–177. (BioMED '08).

NEW ZEALAND DERMATOLOGICAL SOCIETY INCORPORATED. **Idiopathic guttate hypomelanosis**. 2011.

NEW ZEALAND DERMATOLOGICAL SOCIETY INCORPORATED. **DermNet NZ**. 2013.

NIELSEN, K. et al. Retrieval of the physiological state of human skin from UV-Vis reflectance spectra - A feasibility study. **Journal of Photochemistry and Photobiology B: Biology**, [S.l.], v.93, n.1, p.23 – 31, 2008.

NORDLUND, J. et al. (Ed.). **The Pigmentary System**: physiology and pathophysiology. 2.ed. [S.l.]: Blackwell Pub., 2006.

OHSHIMA, H. et al. Melanin and facial skin fluorescence as markers of yellowish discoloration with aging. **Skin Research and Technology**, [S.l.], v.15, n.4, p.496–502, 2009.

PATWARDHAN, S.; DHAWAN, A.; RELUE, P. Monte Carlo simulation of light-tissue interaction: three-dimensional simulation for trans-illumination-based imaging of skin lesions. **Biomedical Engineering, IEEE Transactions on**, [S.l.], v.52, n.7, p.1227–1236, 2005.

RAMANATHAN, N.; CHELLAPPA, R. Modeling shape and textural variations in aging faces. In: AUTOMATIC FACE & GESTURE RECOGNITION, 2008. FG'08. 8TH IEEE INTERNATIONAL CONFERENCE ON. **Anais...** [S.l.: s.n.], 2008. p.1–8.

SCHERBAUM, K. et al. Prediction of Individual Non-Linear Aging Trajectories of Faces. In: COMPUTER GRAPHICS FORUM. **Anais...** [S.l.: s.n.], 2007. v.26, n.3, p.285–294.

SCHMID-SAUGEONA, P.; GUILLODB, J.; THIRANA, J. Towards a computer-aided diagnosis system for pigmented skin lesions. **Computerized Medical Imaging and Graphics**, [S.l.], v.27, n.1, p.65–78, 2003.

SCHWARTZ, R. A.; OKULICZ, J. F.; JOZWIAK, S. **Lentigo**. 2012.

SEN, S.; GHOSH, P.; RAY, D. S. Reaction-diffusion systems with stochastic time delay in kinetics. **Physical Review E**, [S.l.], v.81, n.5, 2010.

SHE, Z. et al. Simulation and analysis of optical skin lesion images. **Skin Research and Technology**, [S.l.], v.12, n.2, p.133–144, 2006.

SI, H.; KONG, D.; YIN, B. Synthesis of 3D Aging Faces Based on Color Gabor Wavelet and Texture Transplant. In: COMPUTATIONAL INTELLIGENCE AND SOFTWARE ENGINEERING, 2009. CISE 2009. INTERNATIONAL CONFERENCE ON. **Anais...** [S.l.: s.n.], 2009. p.1–4.

SILVA, S. F. d.; CALHEIROS, D. B. **Dermatology Atlas**. 2013.

SOCIEDADE BRASILEIRA DE DERMATOLOGIA. **Censo Dermatológico da SBD**. 2006.

SPICER, C. The theory of bacterial constant growth apparatus. **Biometrics**, [S.l.], v.11, n.2, p.225–230, 1955.

STOECKER, W. V.; LI, W. W.; MOSS, R. H. Automatic detection of asymmetry in skin tumors. **Computerized Medical Imaging and Graphics**, [S.l.], v.16, n.3, p.191–197, 1992.

SUO, J. et al. A compositional and dynamic model for face aging. **Pattern Analysis and Machine Intelligence, IEEE Transactions on**, [S.l.], v.32, n.3, p.385–401, 2010.

TAKIWAKI, H. et al. Graphic analysis of the relationship between skin colour change and variations in the amounts of melanin and haemoglobin. **Skin Research and Technology**, [S.l.], v.8, p.78–83, 2002.

TIDDEMAN, B.; STIRRAT, M.; PERRETT, D. Towards realism in facial image transformation: results of a wavelet mrf method. In: COMPUTER GRAPHICS FORUM. **Anais...** [S.l.: s.n.], 2005. v.24, n.3, p.449–456.

TOST, T. **Physikalisch basierte Beleuchtungssimulation von menschlicher Haut in Echtzeit**. 2005. Tese (Doutorado em Ciência da Computação) — Fachhochschule Erfurt.

TURING, A. M. The chemical basis of morphogenesis. **Philosophical Transactions of the Royal Society of London**, [S.l.], v.237, p.37–72, 1952.

TURK, G. **Texturing Surfaces Using Reaction-Diffusion**. 1992. Tese (Doutorado em Ciência da Computação) — The University of North Carolina.

UCHIYAMA, H. et al. Artistically-based technique for aging of the facial modeling. In: DIGITAL INTERACTIVE MEDIA IN ENTERTAINMENT AND ARTS, 2. **Proceedings...** [S.l.: s.n.], 2007. p.187–187.

USATINE, R. P. **Interactive Dermatology Atlas**. 2009.

VERROS, C. D. **Hellenic Dermatological Atlas**. 2013.

WANG, W. et al. Pattern formation of a predator–prey system with Ivlev-type functional response. **Ecological Modelling**, [S.l.], v.221, n.2, p.131–140, 2010.

WHITBOURNE, S. **Adult Development and Aging**: biopsychosocial perspectives. [S.l.]: Wiley, 2007.

WINNEMÖLLER, H. et al. Texture design and draping in 2d images. In: COMPUTER GRAPHICS FORUM. **Anais...** [S.l.: s.n.], 2009. v.28, n.4, p.1091–1099.

WITKIN, A.; KASS, M. Reaction-diffusion textures. **ACM Siggraph Computer Graphics**, [S.l.], v.25, n.4, p.299–308, 1991.

WU, Y.; BEYLOT, P.; MAGNENAT THALMANN, N. Skin aging estimation by facial simulation. In: COMPUTER ANIMATION, 1999. PROCEEDINGS. **Anais...** [S.l.: s.n.], 1999. p.210–219.

WU, Y. et al. Simulating wrinkles and skin aging. **The visual computer**, [S.l.], v.15, n.4, p.183–198, 1999.

WU, Y.; KALRA, P.; THALMANN, N. Physically-based wrinkle simulation & skin rendering. In: EUROGRAPHICS WORKSHOP ON COMPUTER ANIMATION AND SIMULATION. **Anais...** [S.l.: s.n.], 1997. v.97, p.66–79.

WU, Y.; MAGNENAT THALMANN, N.; THALMANN, D. A plastic-visco-elastic model for wrinkles in facial animation and skin aging. In: PACIFIC CONFERENCE ON FUNDAMENTALS OF COMPUTER GRAPHICS, River Edge, NJ, USA. **Proceedings...** World Scientific Publishing Co.: Inc., 1994. p.201–213. (Pacific Graphics '94).

ZHOU, Y. et al. A new method describing border irregularity of pigmented lesions. **Skin Research and Technology**, [S.l.], v.16, n.1, p.66–76, 2010.

ZHOU, Y. et al. Using 3D differential forms to characterize a pigmented lesion in vivo. **Skin Research and Technology**, [S.l.], v.16, n.1, p.77–84, 2010.